

December 2003

**Wigner quasi-probability distribution for the infinite square well:
energy eigenstates and time-dependent wave packets**

M. Belloni*

Physics Department

Davidson College

Davidson, NC 28035 USA

M. A. Doncheski†

Department of Physics

The Pennsylvania State University

Mont Alto, PA 17237 USA

R. W. Robinett‡

Department of Physics

The Pennsylvania State University

University Park, PA 16802 USA

(Dated: October 24, 2018)

arXiv:quant-ph/0312086v1 9 Dec 2003

Abstract

We calculate the Wigner quasi-probability distribution for position and momentum, $P_W^{(n)}(x, p)$, for the energy eigenstates of the standard infinite well potential, using both x - and p -space stationary-state solutions, as well as visualizing the results. We then evaluate the time-dependent Wigner distribution, $P_W(x, p; t)$, for Gaussian wave packet solutions of this system, illustrating both the short-term semi-classical time dependence, as well as longer-term revival and fractional revival behavior and the structure during the collapsed state. This tool provides an excellent way of demonstrating the patterns of highly correlated Schrödinger-cat-like ‘mini-packets’ which appear at fractional multiples of the exact revival time.

*Electronic address: mabelloni@davidson.edu

†Electronic address: mad10@psu.edu

‡Electronic address: rick@phys.psu.edu

I. INTRODUCTION

The solution and visualization of problems in one-dimensional quantum mechanics focuses most often on calculations of the position-space wavefunction, $\psi(x, t)$. More occasionally, problems may be solved using, or transformed into, the momentum-space counterpart, $\phi(p, t)$, using the standard Fourier transforms,

$$\psi(x, t) = \frac{1}{\sqrt{2\pi\hbar}} \int_{-\infty}^{+\infty} \phi(p, t) e^{+ipx/\hbar} dp \quad (1)$$

and

$$\phi(p, t) = \frac{1}{\sqrt{2\pi\hbar}} \int_{-\infty}^{+\infty} \psi(x, t) e^{-ipx/\hbar} dx. \quad (2)$$

Connections between the classical and quantum descriptions of model systems can then be made in a variety of ways. For example, the quantum mechanical expectation values, $\langle x \rangle_t$ and $\langle p \rangle_t$ can be compared to their classical analogs, $x(t)$ and $p(t) = mv(t)$, via Ehrenfest's principle, e.g., $\langle p \rangle_t = m d\langle x \rangle_t / dt$. Quantum mechanical probability densities, $P_{QM}^{(n)}(x) = |\psi_n(x)|^2$ and $P_{QM}^{(n)}(p) = |\phi_n(p)|^2$, can be related to classical probability distributions, calculated using simple “*how long does a particle spend in a given dx or dp interval?*” arguments, or justified in more detail through the WKB approximation.

The visualization of solutions to problems in classical mechanics through a phase-space description, i.e., parametric plots of $p(t)$ versus $x(t)$, is often helpful. It is natural to wonder if a quantum mechanical analog of a phase-space probability distribution, a joint $P(x, p)$ probability density, is a useful construct, despite the obvious problems raised by the Heisenberg uncertainty principle and its connection between x and p .

Wigner [1] was one of the first to address this issue and introduced a quasi- or pseudo-probability distribution corresponding to a general quantum state, $\psi(x, t)$, defined by

$$P_W(x, p; t) \equiv \frac{1}{\pi\hbar} \int_{-\infty}^{+\infty} \psi^*(x + y, t) \psi(x - y, t) e^{2ipy/\hbar} dy. \quad (3)$$

The properties of the Wigner distribution have been discussed in a number of accessible reviews [2] - [10], analyzed for theoretical consistency [11] - [14], used for a number of physical applications [15] - [19], discussed in the pedagogical literature [20] - [25], and have even made the occasional brief appearance in quantum mechanics textbooks [26], [27]. Similar topics are often discussed in the context of both the signal analysis of time-varying spectra [28] (where the two complementary variables are t and ω) and quantum optics [29], [30].

Of all of the familiar model systems often used as tractable pedagogical examples for the application of quantum mechanical techniques, many of the standard potentials have been analyzed in detail using the Wigner distribution, including the harmonic oscillator, linear potential, Morse potential, hydrogen atom (Coulomb problem), and others. The most familiar example of all, however, the infinite square well (ISW) problem, has received less attention [9], [10], [24]. The Wigner function has recently been used to help explain the interesting patterns of probability density, $P(x, t) = |\psi(x, t)|^2$ versus (x, t) , when plotted over long time periods (namely, over the interval $0 < t < T_{rev}$ where T_{rev} is the revival time, to be discussed below). Such patterns have come to be known as quantum carpets [31] - [39]. The authors of Ref. [40] have produced video sequences of the free evolution of an array of Wigner functions constructed from an antisymmetric wavefunction of a wave packet and its mirror wave packet in order to understand the ‘weaving’ of quantum carpets. While such graphical representations of the long-term time dependence of this familiar problem are very interesting, the necessary background material which would allow students (or instructors) to approach such problems themselves has not been stressed.

The purpose of this paper, therefore, is to thoroughly review the derivation of the Wigner distribution for this very accessible problem, not only for individual energy eigenstates, but for time-dependent wave packet solutions. This last case is important as the Wigner function provides a very useful tool for the visualization of the non-trivial long-term time evolution of initially localized wave packets, including revival and fractional revival behaviors. (For a pedagogical review of this topic, see Ref. [41], and for a recent survey of the research literature, see Ref. [42].)

In the next section, we provide a short, self-contained review of many of the general properties of the Wigner quasi-probability distribution, followed in Section III by a collection of useful results for the ISW energy eigenfunctions, in both position and momentum space, helpful for the evaluation of the Wigner function for the ISW. We briefly review the classical phase-space description of the infinite square well in Sec. IV, and in Section V we exhibit the Wigner distribution, $P_W^{(n)}(x, p)$, for the ISW eigenstates, illustrating their derivations in both x - and p -space, and comparing them to their classical counterparts. In Section VI, we extend these results to general wave packet solutions of the infinite square well, focusing on the structure of the Wigner function for time-dependent Gaussian wave packet solutions of the ISW, at a number of full and fractional revivals, as well as during the so-called collapsed

phase, illustrating the power of this method for the visualization of time-dependent quantum phenomena. Throughout, we focus on providing explicit analytic results which can be used for further numerical or visual investigations.

II. REVIEW OF THE WIGNER QUASI-PROBABILITY DISTRIBUTION

The definition of the Wigner function,

$$P_W(x, p; t) \equiv \frac{1}{\pi\hbar} \int_{-\infty}^{+\infty} \psi^*(x+y, t) \psi(x-y, t) e^{2ipy/\hbar} dy, \quad (4)$$

using position-space wavefunctions, can be easily rewritten in momentum space, using Eqn. (2), in the equivalent form

$$P_W(x, p; t) = \frac{1}{\pi\hbar} \int_{-\infty}^{+\infty} \phi^*(p+q, t) \phi(p-q, t) e^{-2iqx/\hbar} dq. \quad (5)$$

The Wigner distribution is easily shown to be real,

$$\begin{aligned} [P_W(x, p; t)]^* &= \frac{1}{\pi\hbar} \int_{-\infty}^{+\infty} \psi(x+y, t) \psi^*(x-y, t) e^{-2ipy/\hbar} dy \\ &= \frac{1}{\pi\hbar} \int_{-\infty}^{+\infty} \psi^*(x+\bar{y}, t) \psi(x-\bar{y}, t) e^{+2ip\bar{y}/\hbar} d\bar{y} \\ &= P_W(x, p; t) \end{aligned} \quad (6)$$

by using a simple change of variables ($\bar{y} = -y$). This is, of course, one of the desired properties of a probability distribution.

Integration of $P_W(x, p; t)$ over one variable or the other is seen to give the correct marginal probability distributions for x and p separately, since

$$\int_{-\infty}^{+\infty} P_W(x, p; t) dp = |\psi(x, t)|^2 = P_{QM}(x, t) \quad (7)$$

$$\int_{-\infty}^{+\infty} P_W(x, p; t) dx = |\phi(p, t)|^2 = P_{QM}(p, t) \quad (8)$$

where one uses the definition of the Dirac δ function

$$\delta(z) = \frac{1}{2\pi} \int_{-\infty}^{+\infty} e^{ikz} dk \quad (9)$$

in Eqns. (4) or (5). This property of $P_W(x, p)$ is clearly another necessary condition for a joint probability density.

However, one can also easily show that the Wigner distributions for two distinct quantum states, $\psi(x, t)$ and $\chi(x, t)$,

$$P_W^{(\psi)}(x, p; t) = \frac{1}{\pi\hbar} \int_{-\infty}^{+\infty} \psi^*(x+y, t) \psi(x-y, t) e^{2ipy/\hbar} dy \quad (10)$$

$$P_W^{(\chi)}(x, p; t) = \frac{1}{\pi\hbar} \int_{-\infty}^{+\infty} \chi^*(x+z, t) \chi(x-z, t) e^{2ipz/\hbar} dz \quad (11)$$

satisfy the relation

$$\int_{-\infty}^{+\infty} dx \int_{-\infty}^{+\infty} dp P_W^{(\psi)}(x, p; t) P_W^{(\chi)}(x, p; t) = \frac{2}{\pi\hbar} |\langle \psi | \chi \rangle|^2. \quad (12)$$

So, for example, if ψ and χ are orthogonal states so that $\langle \psi | \chi \rangle = 0$, it cannot be true that the corresponding Wigner distributions can be everywhere non-negative, as there must be cancellations in the integral in Eqn. (12). The fact that $P_W(x, p; t)$ can be negative is easily confirmed by direct calculation, for example, with simple cases such as the harmonic oscillator (for any $n \geq 1$ state). This feature is, after all, hardly surprising because of the non-commutativity of x and p encoded in the uncertainty principle. Despite this apparent drawback [43], the Wigner function is still useful for the visualization of the correlated position- and momentum-space behavior of quantum eigenstates and wave packets.

A useful benchmark example of the Wigner function is for a Gaussian free-particle wave packet, where the time-dependent momentum- and position-space wavefunctions (for arbitrary initial x_0 and p_0) can be written in the forms

$$\phi_{(G)}(p, t) = \sqrt{\frac{\alpha}{\sqrt{\pi}}} e^{-\alpha^2(p-p_0)^2/2} e^{-ipx_0/\hbar} e^{-ip^2t/2m\hbar} \quad (13)$$

$$\psi_{(G)}(x, t) = \frac{1}{\sqrt{\sqrt{\pi}\alpha\hbar(1+it/t_0)}} e^{ip_0(x-x_0)/\hbar} e^{-ip_0^2t/2m\hbar} e^{-(x-x_0-p_0t/m)^2/2(\alpha\hbar)^2(1+it/t_0)} \quad (14)$$

which are related by Eqns. (1) and (2). These solutions are, of course, well-known to be characterized by

$$\langle p \rangle_t = p_0, \quad \Delta p_t = \frac{1}{\alpha\sqrt{2}} \quad (15)$$

$$\langle x \rangle_t = (p_0/m)t + x_0, \quad \Delta x_t = (\hbar\alpha/\sqrt{2}) \sqrt{1 + (t/t_0)^2} \quad (16)$$

where $t_0 \equiv m\hbar\alpha^2$ is the spreading time. The corresponding Wigner function is easily obtained [8], using standard Gaussian integrals, and is given by

$$P_W^{(G)}(x, p; t) = \frac{1}{\pi\hbar} e^{-\alpha^2(p-p_0)^2} e^{-(x-x_0-pt/m)^2/\beta^2} \quad (17)$$

where $\beta \equiv \hbar\alpha$. In this case, the ultra-smooth Gaussian solution does give a positive-definite $P_W(x, p; t)$ and it is known [44] that such solutions are the only forms which give rise to non-negative Wigner functions.

Another result which will prove useful in what follows is the expression for the Wigner function for the case of a linear combination of two 1-D Gaussians, characterized by different values of x_0 and p_0 . For example, if we assume that at some instant of time we have

$$\begin{aligned} \psi^{(A,B)}(x) &= \gamma\psi_{(G)}(x; x_A, p_A) + \delta\psi_{(G)}(x; x_B, p_B) \\ &= \gamma \left[\frac{1}{\sqrt{\beta}\sqrt{\pi}} e^{-(x-x_A)^2/2\beta^2} e^{ip_A(x-x_A)/\hbar} \right] + \delta \left[\frac{1}{\sqrt{\beta}\sqrt{\pi}} e^{-(x-x_B)^2/2\beta^2} e^{ip_B(x-x_B)/\hbar} \right], \end{aligned} \quad (18)$$

the corresponding Wigner function is given by

$$\begin{aligned} P_W^{(A,B)} &= \frac{1}{\pi\hbar} \left[|\gamma|^2 e^{-\alpha^2(p-p_A)^2} e^{-(x-x_A)^2/\beta^2} + |\delta|^2 e^{-\alpha^2(p-p_B)^2} e^{-(x-x_B)^2/\beta^2} \right. \\ &\quad \left. + 2e^{-\alpha^2(p-\bar{p})^2} e^{-(x-\bar{x})^2/\beta^2} \text{Re} \left\{ \gamma\delta^* e^{i(x_A p_B - x_B p_A)/\hbar} e^{-i(x_A - x_B)(p-\bar{p})/\hbar} e^{i(p_A - p_B)x/\hbar} \right\} \right] \end{aligned} \quad (19)$$

where

$$\bar{x} \equiv \frac{x_A + x_B}{2} \quad \text{and} \quad \bar{p} \equiv \frac{p_A + p_B}{2}. \quad (20)$$

In this case, the Wigner function is characterized by two smooth ‘lumps’ in phase space, corresponding to the values of (x_A, p_A) and (x_B, p_B) of the individual Gaussians, but also by an oscillatory term, centered at a point in phase space defined by the average of these values; the oscillations appear in the x variable (if $p_A \neq p_B$), the p variable (if $x_A \neq x_B$) or both. (A similar expression for the case where $p_A = p_B = 0$ is given in Ref. [27]; see also Refs. [28] and [30] for related examples involving time-frequency analysis and coherent states, respectively.)

For a single stationary state or energy-eigenfunction solution, corresponding to a quantized bound state, given by

$$\psi_n(x, t) = u_n(x) e^{-iE_n t/\hbar} \quad (21)$$

where $u_n(x)$ can be considered as a purely *real* function, the Wigner distribution is time independent

$$P_W^{(n)}(x, p; t) = \frac{1}{\pi\hbar} \int_{-\infty}^{+\infty} u_n(x+y) u_n(x-y) e^{2ipy/\hbar} dy = P_W^{(n)}(x, p). \quad (22)$$

For such solutions, another change of variables argument suffices to show that

$$P_W^{(n)}(x, -p) = P_W^{(n)}(x, +p) \quad (23)$$

which corresponds to the classical result that a particle undergoing bound state motion will spend equal amounts of time with $+p$ (motion to the right) as in the $-p$ direction (going to the left). A more familiar version of this is often discussed in textbooks, where for real eigenstates one knows that

$$\phi_n(p) = \frac{1}{\sqrt{2\pi\hbar}} \int_{-\infty}^{+\infty} u_n(x) e^{-ipx/\hbar} dx \quad (24)$$

$$= \frac{1}{\sqrt{2\pi\hbar}} \int_{-\infty}^{+\infty} u_n(x) [\cos(px/\hbar) - i \sin(px/\hbar)] dx \quad (25)$$

$$\equiv A(p) - iB(p) \quad (26)$$

where $A(p), B(p)$ are then purely real functions. This immediately implies that

$$|\phi_n(-p)|^2 = |A(p) + iB(p)|^2 = [A(p)]^2 + [B(p)]^2 = |A(p) - iB(p)|^2 = |\phi_n(+p)|^2. \quad (27)$$

The general expression for a wave packet solution constructed from such energy eigenstates is

$$\psi(x, t) = \sum_{n=1}^{\infty} a_n u_n(x) e^{-iE_n t/\hbar} \quad (28)$$

where the expansion coefficients satisfy $\sum_n |a_n|^2 = 1$. The time-dependent Wigner distribution for this case is then

$$\begin{aligned} P_W^{(\psi)}(x, p; t) &\equiv \frac{1}{\pi\hbar} \int_{-\infty}^{+\infty} \psi^*(x+y, t) \psi(x-y, t) e^{2ipy/\hbar} dy \\ &= \sum_{m=1}^{\infty} \sum_{n=1}^{\infty} [a_m]^* a_n e^{i(E_m - E_n)t/\hbar} \left[\frac{1}{\pi\hbar} \int_{-\infty}^{+\infty} u_m(x+y) u_n(x-y) e^{2ipy/\hbar} dy \right] \\ &\equiv \sum_{m=1}^{\infty} \sum_{n=1}^{\infty} [a_m]^* a_n e^{i(E_m - E_n)t/\hbar} P_W^{(m,n)}(x, p) \end{aligned} \quad (29)$$

where, in general, we must calculate both diagonal ($m = n$) and off-diagonal ($m \neq n$) terms of the form

$$P_W^{(m,n)}(x, p) = \frac{1}{\pi\hbar} \int_{-\infty}^{+\infty} u_m(x+y) u_n(x-y) e^{2ipy/\hbar} dy. \quad (30)$$

While $P_W^{(\psi)}(x, p; t)$ is real, the off-diagonal Wigner terms are not necessarily so, but do satisfy

$$\left[P_W^{(m,n)}(x, p) \right]^* = P_W^{(n,m)}(x, p). \quad (31)$$

III. INFINITE SQUARE WELL RESULTS IN POSITION AND MOMENTUM SPACE

Because the Wigner function can be evaluated using either position- or momentum-space wavefunctions, we review the properties of, and interconnections between, these solutions for the infinite square well (ISW). The standard problem of a particle of mass m confined by the potential

$$V(x) = \begin{cases} 0 & \text{for } 0 < x < L \\ \infty & \text{otherwise} \end{cases} \quad (32)$$

has energy eigenvalues and position-space eigenfunctions (which are non-zero only within the well) which are given by

$$E_n = \frac{\hbar^2 \pi^2 n^2}{2mL^2} = \frac{p_n^2}{2m} \quad (p_n \equiv n\pi\hbar/L) \quad \text{with} \quad u_n(x) = \sqrt{\frac{2}{L}} \sin\left(\frac{n\pi x}{L}\right). \quad (33)$$

The position-space eigenfunctions have a generalized parity property about the midpoint of the well since

$$u_n(L-x) = \sqrt{\frac{2}{L}} \sin\left(\frac{n\pi(L-x)}{L}\right) = -\sqrt{\frac{2}{L}} \cos(n\pi) \sin\left(\frac{n\pi x}{L}\right) = (-1)^{n+1} u_n(x). \quad (34)$$

As with any such system, the eigenfunctions can be made orthonormal, which in this case can be readily checked explicitly by direct calculation of

$$\begin{aligned} \langle u_m | u_n \rangle &= \left(\frac{2}{L}\right) \int_0^L \sin\left(\frac{m\pi x}{L}\right) \sin\left(\frac{n\pi x}{L}\right) dx \\ &= \left\{ \frac{\sin[(m-n)\pi]}{(m-n)\pi} - \frac{\sin[(m+n)\pi]}{(m+n)\pi} \right\} = \delta_{m,n}. \end{aligned} \quad (35)$$

The momentum-space eigenfunctions are given by Eqn. (2) as

$$\begin{aligned} \phi_n(p) &= \frac{1}{\sqrt{2\pi\hbar}} \int_0^L u_n(x) e^{-ipx/\hbar} dx \\ &= (-i) \sqrt{\frac{L}{\pi\hbar}} e^{-ipL/2\hbar} \left[e^{+in\pi/2} \frac{\sin[(pL/\hbar - n\pi)/2]}{(pL/\hbar - n\pi)} - e^{-in\pi/2} \frac{\sin[(pL/\hbar + n\pi)/2]}{(pL/\hbar + n\pi)} \right] \end{aligned}$$

and the resulting probability density is given by

$$\begin{aligned} |\phi_n(p)|^2 &= \left(\frac{L}{\hbar\pi}\right) \left[\frac{\sin^2[(pL/\hbar - n\pi)/2]}{(pL/\hbar - n\pi)^2} + \frac{\sin^2[(pL/\hbar + n\pi)/2]}{(pL/\hbar + n\pi)^2} \right. \\ &\quad \left. - 2 \cos(n\pi) \frac{\sin[(pL/\hbar - n\pi)/2] \sin[(pL/\hbar + n\pi)/2]}{(pL/\hbar - n\pi)(pL/\hbar + n\pi)} \right] \end{aligned} \quad (36)$$

which will be useful for visualization purposes.

While these forms demonstrate more explicitly the strong peaking of the probability amplitude near the expected values of $p = \pm p_n = \pm n\pi\hbar/L$, they do not make clear the finite extent (limited to the range $[0, L]$) of the position-space amplitude. In order to exemplify this dependence, we can evaluate the inverse Fourier transform, via Eqn. (1), to explicitly obtain $u_n(x)$. Because such calculations will be useful in the evaluation of the Wigner distribution using momentum-space wavefunctions, we examine this seldom-discussed analysis [9] in some detail. We require

$$\begin{aligned}
u_n(x) &= \frac{1}{\sqrt{2\pi\hbar}} \int_{-\infty}^{+\infty} \phi_n(p) e^{ipx/\hbar} dp \\
&= (-i) \sqrt{\frac{L}{2\pi^2\hbar^2}} \left\{ e^{+in\pi/2} \int_{-\infty}^{+\infty} e^{ip(x-L/2)/\hbar} \frac{\sin[(pL/\hbar - n\pi)/2]}{(pL/\hbar - n\pi)} dp \right. \\
&\quad \left. - e^{-in\pi/2} \int_{-\infty}^{+\infty} e^{ip(x-L/2)/\hbar} \frac{\sin[(pL/\hbar + n\pi)/2]}{(pL/\hbar + n\pi)} dp \right\} \\
&\equiv (-i) \sqrt{\frac{L}{2\pi^2\hbar^2}} \{ e^{+in\pi/2} I_A - e^{-in\pi/2} I_B \} .
\end{aligned} \tag{37}$$

Each integral, I_A, I_B , can be done in turn using a change of variables, giving, for example,

$$\begin{aligned}
I_A &= \int_{-\infty}^{+\infty} e^{ip(x-L/2)/\hbar} \frac{\sin[(pL/\hbar - n\pi)/2]}{(pL/\hbar - n\pi)} dp \\
&= \left(\frac{\hbar}{L}\right) e^{+in\pi x/L} e^{-in\pi/2} \int_{-\infty}^{+\infty} \frac{\sin(q)}{q} e^{imq} dq \\
&= \left(\frac{\hbar}{L}\right) e^{+in\pi x/L} e^{-in\pi/2} \int_{-\infty}^{+\infty} \frac{\sin(q)}{q} [\cos(mq) + i \sin(mq)] dq
\end{aligned} \tag{38}$$

where we have used

$$q \equiv \frac{1}{2} \left(\frac{pL}{\hbar} - n\pi \right) \quad \text{and} \quad m \equiv \frac{(2x - L)}{L} . \tag{39}$$

The piece of I_A which includes the $\sin(mq)$ term vanishes for symmetry reasons (odd integrand over a symmetric interval), while the component with $\cos(mq)$ can be done using standard handbook [45] results, which we review in Appendix A. The result is

$$\int_{-\infty}^{+\infty} \frac{\sin(q)}{q} \cos(mq) dq = \begin{cases} \pi & \text{for } m^2 < 1 \\ \pi/2 & \text{for } m^2 = 1 \\ 0 & \text{for } m^2 > 1 \end{cases} \tag{40}$$

The restriction on m corresponds to

$$m^2 = \left(\frac{2x - L}{L} \right)^2 < 1 \quad \longrightarrow \quad -1 < \frac{2x - L}{L} < +1 \quad \longrightarrow \quad 0 < x < L \tag{41}$$

which explicitly demonstrates the finite extent of the position-space wavefunction which is non-vanishing only in the range $[0, L]$, as expected. Performing the second integral (I_B) in the same way, and combining factors, we find that the non-vanishing position-space wavefunction is given by

$$\begin{aligned} u_n(x) &= (-i)\sqrt{\frac{L}{2\pi^2\hbar^2}}\left(\frac{\hbar\pi}{L}\right)\{e^{+in\pi/2}e^{+in\pi x/L}e^{-in\pi/2} - e^{-in\pi/2}e^{-in\pi x/L}e^{+in\pi/2}\} \\ &= \sqrt{\frac{2}{L}}\sin\left(\frac{n\pi x}{L}\right) \quad \text{for } 0 < x < L \end{aligned} \quad (42)$$

again, as expected. For future notational convenience, we can write this in the form

$$u_n(x) = \sqrt{\frac{2}{L}}\sin\left(\frac{n\pi x}{L}\right)\mathcal{R}(x; 0, L) \quad (43)$$

where

$$\mathcal{R}(x; a, b) = \begin{cases} 0 & \text{for } x < a, x > b \\ 1/2 & \text{for } x = a, x = b \\ 1 & \text{for } a < x < b \end{cases} . \quad (44)$$

(We note that the results from Eqns. (40), (43), and (44) can also be expressed in terms of the Heaviside step-function, $\Theta(\xi)$, as, for example in Ref. [24].

Just as in position space, it is possible to explicitly demonstrate the orthonormality of the momentum-space eigenfunctions, by calculating $\langle\phi_m|\phi_n\rangle$. Since similar methods will also be useful in what follows, we illustrate one typical step in such an evaluation. One required integral, for example, is given by

$$\mathcal{I} = \left(\frac{L}{\pi\hbar}\right)e^{i(n-m)\pi/2}\int_{-\infty}^{+\infty}\frac{\sin[(pL/\hbar - m\pi)/2]\sin[(pL/\hbar - n\pi)/2]}{(pL/\hbar - m\pi)(pL/\hbar - n\pi)}dp \quad (45)$$

The denominator can be written in a form which allows use of standard integrals, namely

$$\frac{1}{(pL/\hbar - m\pi)(pL/\hbar - n\pi)} = \frac{1}{(m - n)\pi}\left[\frac{1}{(pL/\hbar - m\pi)} - \frac{1}{(pL/\hbar - n\pi)}\right]. \quad (46)$$

Appropriate changes of variables and integrals as in Eqn. (40) then give simple closed form expressions, and the complete result for $\langle\phi_m|\phi_n\rangle$ is the indeed same as in Eqn. (35).

Finally, for eventual comparison to the Wigner distributions for the ISW, we plot some standard representations of the position- and momentum-space probability densities for two low-lying states ($n = 1, 10$) in Fig. 1.

IV. CLASSICAL PHASE-SPACE PICTURE OF THE INFINITE SQUARE WELL

Phase-space plots of the motion of classical mechanical systems are increasingly stressed in undergraduate textbooks on the subject, perhaps because of their utility in the analysis or visualization of classically chaotic systems. The correlated time dependence of $x(t)$ and $p(t)$ in such systems is indeed easily and usefully visualized by parametric plots in the $x - p$ plane, and the most familiar example is perhaps the case of the harmonic oscillator. For this case, the most general form of the solution can be written in the form

$$x(t) = x_A \cos(\omega t + \phi) \quad \text{and} \quad p(t) = -m\omega x_A \sin(\omega t + \phi) \equiv p_A \sin(\omega t + \phi) \quad (47)$$

and the constant value of the total energy is

$$\frac{[p(t)]^2}{2m} + \frac{1}{2}m\omega[x(t)]^2 = E = \frac{1}{2}m\omega^2 x_A^2 = \frac{p_A^2}{2m}. \quad (48)$$

This defines the elliptical phase-space path followed by the particle, and a classical description of the joint probability densities requires that the particle be restricted to this path, namely, that

$$P_{CL}(x, p) \propto \delta(E - p^2/2m - m\omega^2 x^2/2). \quad (49)$$

For the classical infinite square well, the situation is at once conceptually simpler, but somewhat more subtle mathematically. The classical paths consist of simple ‘back-and-forth’ motion, at constant speed ($p = \pm p_0 = \pm\sqrt{2mE}$) with sudden (discontinuous) jumps at the walls ($x = 0, L$). This is illustrated in Fig. 2 with (solid) horizontal lines at $\pm p_0$ connected by (dashed) vertical ‘jumps’ at the walls. The classical joint probability distribution can then be described intuitively as

$$P_{CL}(x, p) \propto \delta(E - p^2/2m) \quad \text{for } 0 < x < L \quad (50)$$

and the corresponding classical probability densities for position, $P_{CL}(x)$, and momentum, $P_{CL}(p)$, are obtained by integrating over one variable or the other, as in Eqns. (7) and (8). For the p -space probability density, since there is no explicit x dependence inside the δ -function, one finds that

$$P_{CL}(p) \propto \int \delta(E - p^2/2m) dx \propto \delta(E - p^2/2m) \propto \frac{1}{2p_0} [\delta(p - p_0) + \delta(p + p_0)]. \quad (51)$$

When properly normalized this reduces to

$$P_{CL}(p) = \frac{1}{2} [\delta(p - p_0) + \delta(p + p_0)] \quad (52)$$

or equal probabilities of finding the particle with $p = \pm p_0$. The corresponding position-space probability

$$P_{CL}(x) \propto \int \delta(E - p^2/2m) dp \propto \text{constant independent of } x \quad (53)$$

for $0 < x < L$, or when properly normalized gives

$$P_{CL}(x) = \frac{1}{L} \quad \text{for } 0 < x < L. \quad (54)$$

These classical values are also shown in Fig. 2 (dashed horizontal line for $P_{CL}(x)$ and two vertical dashed ‘spikes’ for $P_{CL}(p)$) to be compared to a large quantum number ($n = 10$) solution of the quantum case for comparison.

V. WIGNER DISTRIBUTION FOR THE INFINITE WELL: EIGENSTATES

For the calculation of the Wigner distribution for energy eigenstates in the ISW, we will first work in position space and use

$$P_W^{(n)}(x, p) = \frac{1}{\pi\hbar} \int u_n(x+y) u_n(x-y) e^{2ipy/\hbar} dy \quad (55)$$

since the position-space eigenstates, $u_n(x)$, can be made purely real. The limits of integration are determined by the restriction that the $u_n(x \pm y)$ are non-vanishing only in the range $[0, L]$, so that we must simultaneously satisfy the requirements

$$0 \leq x + y \leq L \quad \text{and} \quad 0 \leq x - y \leq L. \quad (56)$$

This leads to upper and lower bounds for the integral over y in Eqn. (55) which depend on x via

$$-x \leq y \leq +x \quad \text{for } 0 \leq x \leq L/2 \quad (57)$$

$$-(L-x) \leq y \leq +(L-x) \quad \text{for } L/2 \leq x \leq L. \quad (58)$$

Thus, over the left-half of the allowed x interval, $[0, L/2]$, we have

$$\begin{aligned}
P_W^{(n)}(x, p) &= \frac{1}{\pi\hbar} \int_{-x}^{+x} \left[\sqrt{\frac{2}{L}} \sin\left(\frac{n\pi(x+y)}{L}\right) \right] \left[\sqrt{\frac{2}{L}} \sin\left(\frac{n\pi(x-y)}{L}\right) \right] e^{2ipy/\hbar} dy \\
&= \left(\frac{2}{\pi\hbar L} \right) \left\{ \frac{\sin[2(p/\hbar - n\pi/L)x]}{4(p/\hbar - n\pi/L)} + \frac{\sin[2(p/\hbar + n\pi/L)x]}{4(p/\hbar + n\pi/L)} \right. \\
&\quad \left. - \cos\left(\frac{2n\pi x}{L}\right) \frac{\sin(2px/\hbar)}{(2p/\hbar)} \right\}, \tag{59}
\end{aligned}$$

while over the right-half of the interval, $[L/2, L]$, one makes the replacement $x \rightarrow L-x$. This form has been derived before [9], [10], [24] although in at least one reference it is written in terms of Bessel functions ($j_0(z)$) which somewhat obscures its simple derivation. One can then demonstrate explicitly that

$$\int_0^L P_W^{(n)}(x, p) dx = |\phi_n(p)|^2 \quad \text{and} \quad \int_{-\infty}^{+\infty} P_W^{(n)}(x, p) dp = |u_n(x)|^2 \tag{60}$$

using standard integrals, or ones described in Appendix A.

The evaluation of the Wigner function using momentum-space wavefunctions, using Eqn. (5) integrated over all p -values, is also instructive, as it naturally leads to the same restrictions on x as seen in Eqn. (41), as well as the $x \rightarrow L-x$ identification over the two half-intervals, as in Eqn. (58). We exhibit some of the relevant parts of this calculation in Appendix B.

With these results in hand, we exhibit examples of the Wigner function for the ISW, for the $n = 1$ ground state (Figs. 3 and 4) and for an excited ($n = 10$) state (Figs. 5 and 6), using $\hbar = L = 1$ for simplicity. For ease of visualization, for both cases we show separate plots for $P_W^{(n)}(x, p) > 0$ and $P_W^{(n)}(x, p) < 0$ values. For the ground state, the projection of $P_W^{(n)}(x, p)$ onto the x - and p -axes to obtain $|u_n(x)|^2$ and $|\phi_n(p)|^2$ (as in Fig. 1) via Eqn. (60) is straightforward to visualize, and we also note that this relatively smooth ground state wavefunction gives a Wigner distribution which is almost everywhere positive (Fig. 3), but with a small negative contribution as seen most clearly in Fig. 4.

For the $n = 10$ (or any $n \gg 1$) case, the structures are more surprising, but still yield the appropriate probability densities upon projection onto the x - and p -axes. The obvious ‘triangular’ form of both the ‘fin’-shaped features along the $p = \pm p_n$ axes and the central ‘spines’ along the $p = 0$ axes can be easily seen to arise from the form in Eqn. (59) in those limits. For those cases, the $\sin[2Fx/\hbar]/F$ form (where $F = (p - p_n)$, $(p + p_n)$, or p) of each term (for $0 < x < L/2$) gives a linear dependence on x when $F \rightarrow 0$, while for $L/2 < x < L$

this is replaced by the $L - x$ factor, giving the triangular dependence obvious from Fig. 5. The smooth features along the $p = \pm p_n$ axes (seen only for positive values of $P_W^{(n)}(x, p)$) are obviously reminiscent of the classical phase-space picture in Fig. 2, while the highly oscillatory structures ‘inside’ the classical rectangular boundary (obvious in both Figs. 5 and 6) locally average to the small, but non-vanishing values of the cross-term in Eqn. (36) and are just as clearly purely quantum mechanical in origin.

VI. WIGNER DISTRIBUTION FOR THE INFINITE WELL: WAVE PACKET SOLUTIONS

For a general wave packet solution for the infinite square well, we require the on- and off-diagonal terms in Eqn. (30). Using the position-space eigenstates in Eqn. (33), over the interval $[0, L/2]$ we find that

$$\begin{aligned}
P_W^{(m,n)}(x, p) &= \frac{1}{\pi\hbar} \int_{-x}^{+x} \left[\sqrt{\frac{2}{L}} \sin\left(\frac{m\pi(x+y)}{L}\right) \right] \left[\sqrt{\frac{2}{L}} \sin\left(\frac{n\pi(x-y)}{L}\right) \right] e^{2ipy/\hbar} dy \\
&= \frac{1}{\pi\hbar} \left[e^{+i(m-n)\pi x/L} \frac{\sin[(2p/\hbar + (m+n)\pi/L)x]}{2pL/\hbar + (m+n)\pi} \right. \\
&\quad \left. + e^{-i(m-n)\pi x/L} \frac{\sin[(2p/\hbar - (m+n)\pi/L)x]}{2pL/\hbar - (m+n)\pi} \right. \\
&\quad \left. - e^{+i(m+n)\pi x/L} \frac{\sin[(2p/\hbar + (m-n)\pi/L)x]}{2pL/\hbar + (m-n)\pi} \right. \\
&\quad \left. - e^{-i(m+n)\pi x/L} \frac{\sin[(2p/\hbar - (m-n)\pi/L)x]}{2pL/\hbar - (m-n)\pi} \right] \quad (61)
\end{aligned}$$

and it is easy to check that this result reduces to the expression in Eqn. (59) when $m = n$. In order to extend this to the interval $[L/2, L]$, it is important to note that the substitution $x \rightarrow L - x$ should be made *only* in those terms arising from the integration over dy , namely, the $\sin[(2p/\hbar \pm (m \pm n)/L)x]$ terms.

These results can then be used to evaluate the time-dependent Wigner function for any initial wave packet in the infinite square well, with the simplest non-trivial example being that for a two-state system, $\psi(x, 0) = \gamma u_1(x) + \delta u_2(x)$, which can then be compared to more standard representations in position space or momentum space [46]. Such states, while exhibiting non-trivial dynamical behavior (sometimes said to mimic time-dependent radiating systems [47]), are still highly quantum mechanical and to approach the semi-classical limit, we require more localized states, constructed from higher quantum number

eigenfunctions.

We can examine the time dependence of such an initially localized state by choosing a standard Gaussian of the form

$$\psi_{(G)}(x, 0) = \frac{1}{\sqrt{b\sqrt{\pi}}} e^{-(x-x_0)^2/2b^2} e^{ip_0(x-x_0)/\hbar} \quad (62)$$

where we will always assume that x_0 is chosen such that $\psi_{(G)}(x, 0)$ is sufficiently contained within the well so that we make an exponentially small error by neglecting any overlap with the region outside the walls, and may thus also ignore any problems associated with possible discontinuities at the wall. In practice, this condition only requires the wave packet to be a few times $\Delta x_0 = b/\sqrt{2}$ away from an infinite wall boundary. With these assumptions, we can then extend the integration region from the finite $[0, L]$ interval to the entire 1-D space, giving the (exponentially good) approximation for the expansion coefficients [48], [49]

$$\begin{aligned} a_n &= \int_0^L [u_n(x)] [\psi_G(x, 0)] dx \\ &\approx \int_{-\infty}^{+\infty} [u_n(x)] [\psi_G(x, 0)] dx \\ &= \left(\frac{1}{2i}\right) \sqrt{\frac{4b\pi}{L\sqrt{\pi}}} [e^{in\pi x_0/L} e^{-b^2(p_0+n\pi\hbar/L)^2/2\hbar^2} - e^{-in\pi x_0/L} e^{-b^2(p_0-n\pi\hbar/L)^2/2\hbar^2}]. \end{aligned} \quad (63)$$

The position-space and momentum-space wavefunctions are then given by

$$\psi(x, t) = \sum_{n=1}^{\infty} a_n u_n(x) e^{-iE_n t/\hbar} \quad \text{and} \quad \phi(p, t) = \sum_{n=1}^{\infty} a_n \phi_n(p) e^{-iE_n t/\hbar} \quad (64)$$

while the time-dependent Wigner distribution is given by Eqn. (29).

The time dependence of any general quantum state (not necessarily the ISW) is determined by the $\exp(-iE_n t/\hbar)$ factors, and for highly localized, semi-classical wave packets, where one typically can expand $E(n)$ about a (large) central value of the quantum number, $n_0 \gg 1$, one can write this dependence in the form [41], [42]

$$\begin{aligned} e^{-iE_n t/\hbar} &= \exp\left(-i/\hbar \left[E(n_0)t + (n - n_0)E'(n_0)t + \frac{1}{2}(n - n_0)^2 E''(n_0)t \right. \right. \\ &\quad \left. \left. + \frac{1}{6}(n - n_0)^3 E'''(n_0)t + \dots \right] \right) \\ &\equiv \exp\left(-i\omega_0 t - 2\pi i(n - n_0)t/T_{cl} - 2\pi i(n - n_0)^2 t/T_{rev} \right. \\ &\quad \left. - 2\pi i(n - n_0)^3 t/T_{super} + \dots \right) \end{aligned} \quad (65)$$

where each term in the expansion (after the first) defines an important characteristic time scale, via

$$T_{cl} = \frac{2\pi\hbar}{|E'(n_0)|}, \quad T_{rev} = \frac{2\pi\hbar}{|E''(n_0)|/2}, \quad \text{and} \quad T_{super} = \frac{2\pi\hbar}{|E'''(n_0)|/6}, \quad (66)$$

namely, the classical period (T_{cl}), the revival time (T_{rev}), and the super-revival time (T_{super}). The classical periodicity for the ISW in this formalism is given by

$$T_{cl} = \frac{2\pi\hbar}{|E'(n_0)|} = \frac{2mL^2}{\hbar\pi n_0} = \frac{2L}{[(\hbar\pi n_0/L)/m]} = \frac{2L}{v_{n_0}} \quad \text{where} \quad v_{n_0} \equiv \frac{p_{n_0}}{m} \quad (67)$$

and v_{n_0} is the analog of the classical speed, giving a result in agreement with classical expectations. Depending on the relative values of T_{cl} and the spreading time, t_0 , there can be many obvious similarities to the classical motion, easily visualized through an expectation value analysis [50].

As an example of quasi-classical time evolution of a quantum state, we consider a Gaussian wave packet characterized by the parameters

$$2m = L = \hbar = 1 \quad \Delta x_0 = \frac{b}{\sqrt{2}} = \frac{1}{20} \ll 1 = L \quad (68)$$

$$p_0 = +\frac{40\pi\hbar}{L} = 40\pi \gg 10 = \Delta p_0 = \frac{\hbar}{2\Delta x_0} \quad x_0 = L/2 = 0.5. \quad (69)$$

We use a central values of $n_0 = 40$ so that the ratio of classical periodicity to spreading time is $T_{cl}/t_0 = 10/\pi$ and significant spreading can be seen even over half a classical period.

We first show in Fig. 7 the position- and momentum-space probability densities for the initial wave packet ($t = 0$, dashed) and half a classical period later ($t = T_{cl}/2$, solid). The spreading in position space is clearly visible, while the switch from momentum values centered around $+p_0$ to $-p_0$ after the first ‘collision’ with the infinite wall is also apparent. For comparison, we show $P_W(x, p; t)$ for the same two times in Fig. 8 and note the two highly localized ‘lumps’ of probability, centered at the appropriate locations in phase space, but with the obvious spreading in position space, consistent with the form in Eqn. (17), and with positive-definite values in each case. This behavior is similar to the classical phase space picture in Fig. 2 for the two states denoted by squares, separated by $T_{cl}/2$.

For comparison to this quasi-classical behavior, we also show results for $t = T_{cl}/4$, corresponding to the time when the classical particle would ‘hit’ the wall, both for the position- and momentum-space probability densities (in Fig. 9) as well as for the Wigner function

(in Fig. 10). In this case, the description of the time-dependent solution in terms of sums of image states [48], [51], [52] is appropriate, with the large, interference term at $p \approx 0$ in the Wigner distribution arising from effects such as in Eqn. (19). As discussed above, the Wigner function is positive-definite only at times when it can be well approximated as a single isolated Gaussian, such as at $t = 0$ and $t = T_{cl}/2$ in Fig. 8, or, as we will see, at the revival time T_{rev} . As seen here at $T_{cl}/4$, at many other times the Wigner function can become negative and we will henceforth only show the $P_W(x, p; t) > 0$ values for ease of visualization.

For longer time scales, we require the revival time, T_{rev} , which is given by

$$T_{rev} \equiv \frac{2\pi\hbar}{|E''(n_0)|/2} = \frac{2\pi\hbar}{E_0} = \frac{4mL^2}{\hbar\pi} = (2n_0)T_{cl} \quad (70)$$

and for the infinite square well no longer time scales are present due to the purely quadratic dependence of the energy eigenvalues. The revival time scale can clearly be much larger than the classical period for wave packets characterized by $n_0 \gg 1$ (giving $T_{rev}/T_{cl} = 80$ for the examples presented here.)

The quantum revivals for this system are exact since we have

$$\psi(x, t + T_{rev}) = \sum_{n=1}^{+\infty} a_n u_n(x) e^{-iE_n(t+T_{rev})/\hbar} = \sum_{n=1}^{+\infty} a_n u_n(x) e^{-iE_n t/\hbar} e^{-i2\pi n^2} = \psi(x, t) \quad (71)$$

and any wave packet returns to its initial state after a time T_{rev} . At half this time, $t = T_{rev}/2$, the wave packet also reforms [53], since

$$\begin{aligned} \psi(L-x, t + T_{rev}/2) &= \sum_{n=1}^{\infty} a_n u_n(L-x) e^{-iE_n t/\hbar} e^{-iE_n T_{rev}/2\hbar} \\ &= \sum_{n=1}^{\infty} a_n u_n(x) e^{-iE_n t/\hbar} \left[(-1)^{n+1} e^{-in^2\pi} \right] \\ &= -\psi(x, t) \end{aligned} \quad (72)$$

where we have used the symmetry properties of the $u_n(x)$ from Eqn. (34). This implies that

$$|\psi(x, t + T_{rev}/2)|^2 = |\psi(L-x, t)|^2 \quad (73)$$

so that at half a revival time later, any initial wave packet will reform itself (same shape, width, etc.), but at a location mirrored about the center of the well. Using Eqn. (72), one can also show that

$$|\phi(p, t + T_{rev}/2)|^2 = |\phi(-p, t)|^2 \quad (74)$$

so that the packet is moving with ‘mirror’ (opposite) momentum values as well, and therefore in the opposite corner of phase space.

More interestingly, at various fractional multiples of the revival time, pT_{rev}/q , the wave packet can also reform as several small copies (sometimes called ‘mini-packets’ or ‘clones’) of the original wave packet, with well-defined phase relationships. (The original mathematical arguments showing how this behavior arises in general wave packet solutions were made by Averbukh and Perelman in Ref. [54]). For example, near $t \approx T_{rev}/4$ the wave packet can be written as a linear combination of the form

$$\psi(x, t \approx T_{rev}/4) = \frac{1}{\sqrt{2}} [e^{-i\pi/4} \psi_{cl}(x, t) + e^{+i\pi/4} \psi_{cl}(x, t + T_{cl}/2)]$$

where $\psi_{cl}(x, t)$ describes the short-term time development of the initial wave packet obtained by keeping only the terms linear in n in the expansion in Eqn. (65). The position- and momentum-space probability densities at $T_{rev}/4$ are shown in Fig. 11 illustrating this phenomena, but this behavior is much more interestingly visualized through the Wigner function description in Fig. 12. The Wigner function in this case is well-represented by the terms in Eqn. (19), where the cross-term is only oscillatory in the p variable, since the corresponding values of $x_A = x_B = L/2 = x_0$ are the same in this case.

A similar, but even richer, situation can be seen at $T_{rev}/3$, where there are three distinct ‘mini-packets’ in position space, and corresponding interesting interference structure in momentum space, as shown in Fig. 13. The explicit form of the wavefunction near this fractional revival time is given by [54]

$$\psi(x, t \approx T_{rev}/3) = -\frac{i}{\sqrt{3}} [\psi_{cl}(x, t) + e^{2\pi i/3} \{\psi_{cl}(x, t + T_{cl}/3) + \psi_{cl}(x, t + 2T_{cl}/3)\}] \quad (75)$$

and exactly this type of highly correlated state is obvious in the Wigner function visualization in Fig. 14, with three smooth ‘lumps’ corresponding to the diagonal terms in Eqn. (19), and three oscillatory ‘cross-terms’ at the average value locations in phase space predicted by Eqn. (20), with the appropriate ‘wiggleness’.

Finally, at other ‘random’ times during the time evolution of such states, not near any resolvable fractional revivals, the wavefunction collapses to something like an incoherent sum of eigenstates, with little or no obvious correlations. A view of this behavior at such a time (represented here by $t = T^* = 16T_{rev}/37$) using $|\psi(x, t)|^2$ and $|\phi(p, t)|^2$ is shown in Fig. 15, as well as using the Wigner function in Fig. 16.

VII. CONCLUSIONS AND DISCUSSIONS

While the infinite well is one of the most standard model problems in all of introductory quantum mechanics, it continues to be used as a benchmark system for the analysis and visualization of new quantum phenomena, including wave packet revivals. In a similar vein, the Wigner function, which was invented more than 70 years ago, continues to play an important role in the analysis, understanding, and visualization of quantum systems, and in related fields such as signal analysis and quantum optics. We have provided a thorough review of both the analytic structure of the Wigner function for energy eigenstates as well as for time-dependent Gaussian wave packet states for this important exemplary quantum system, focusing on the visualization of wave packet states at fractional revival times. (Additional images not included in this paper can be accessed at <http://webphysics.davidson.edu/mjb/wigner/>.)

Given the relative straightforwardness of the calculations involved here for the ISW, it is easy to imagine extending the results presented here to simple extensions, such as a finite square well, or an asymmetric infinite well of the form

$$V(x) = \begin{cases} +\infty & \text{for } x < -b \\ 0 & \text{for } -b < x < 0 \\ +V_0 & \text{for } 0 < x < +a \\ +\infty & \text{for } +a < x \end{cases} . \quad (76)$$

This last form is interesting as the eigenstates exhibit less trivial correlations between the magnitude/wiggleness of the position-space wavefunction (due to the varying classical speeds in the two sides of the well) which can then be connected to the behavior in momentum space more directly using the Wigner function. This example is also instructive since, because of the unphysical discontinuity of the potential, there are typically surprising results [55] when one compares quantum results to classical expectations for position- and momentum-space probability densities. This type of asymmetric well is also of the form for which coherent charge oscillations have been observed experimentally [56], consisting of a two state system,

$$\psi(x, t) = \gamma [u_n(x)e^{-iE_a t/\hbar}] + \delta [u_b(x)e^{-iE_b t/\hbar}] \quad (77)$$

with $E_a < V_0$ and $E_b > V_0$.

Acknowledgments We would like to thank Wolfgang Christian and Tim Gfroerer for useful conversations regarding this work. MB was supported in part by a Research Corporation Cottrell College Science Award (CC5470) and the National Science Foundation (DUE-0126439).

APPENDIX A: TRIGONOMETRIC INTEGRALS

For many of the calculations included here, we require versions of the integral

$$\int_{-\infty}^{+\infty} \frac{\sin(z) \cos(mz)}{z} dz = \begin{cases} 0 & \text{for } m < -1 \text{ and } m > +1 \\ \pi/2 & \text{for } m = \pm 1 \\ \pi & \text{for } m^2 < 1 \end{cases} \quad (\text{A1})$$

which is a handbook [45] result. We can briefly justify these results, starting with the single integral

$$\int_{-\infty}^{+\infty} \frac{\sin(z)}{z} dz = \pi \quad (\text{A2})$$

which itself can be derived using contour integration. This can be generalized to

$$\int_{-\infty}^{+\infty} \frac{\sin(mz)}{z} dz = \begin{cases} +\pi & \text{for } m > 0 \\ 0 & \text{for } m = 0 \\ -\pi & \text{for } m < 0 \end{cases} \quad (\text{A3})$$

by a change of variables, and considering the special $m = 0$ case separately. The general integral in Eqn. (A1) can then be obtained by writing

$$\sin(z) \cos(mz) = \frac{1}{2} \{ \sin[(1+m)z] + \sin[(1-m)z] \} \quad (\text{A4})$$

and using Eqn. (A3) twice. The special case of $m = 1$ is done by noting that

$$\int_{-\infty}^{+\infty} \frac{\sin(z) \cos(z)}{z} dz = \int_{-\infty}^{+\infty} \frac{\sin(2z)}{2z} dx = \frac{1}{2} \int_{-\infty}^{+\infty} \frac{\sin(w)}{w} dw = \frac{\pi}{2} \quad (\text{A5})$$

where $w = 2z$ and a simple trig identity is used. Another integral that is useful for normalization calculations is

$$\int_{-\infty}^{+\infty} \frac{\sin^2(z)}{z^2} dz = \pi \quad (\text{A6})$$

which is another handbook result derivable using contour integration techniques.

APPENDIX B: WIGNER DISTRIBUTION FROM MOMENTUM-SPACE WAVEFUNCTIONS

The evaluation of the Wigner function, using momentum-space wavefunctions as in Eqn. (5), requires the integral

$$\begin{aligned}
P_W^{(n)}(x, p) &= \left(\frac{L}{(\pi\hbar)^2} \right) \int_{-\infty}^{+\infty} dq e^{-2iqx/\hbar} e^{+i(p+q)L/2\hbar} e^{-i(p-q)L/2\hbar} \\
&\times \left\{ e^{-in\pi/2} \frac{\sin[((p+q)L/\hbar - n\pi)/2]}{[(p+q)L/\hbar - n\pi]} - e^{+in\pi/2} \frac{\sin[((p+q)L/\hbar + n\pi)/2]}{[(p+q)L/\hbar + n\pi]} \right\} \\
&\times \left\{ e^{+in\pi/2} \frac{\sin[((p-q)L/\hbar - n\pi)/2]}{[(p-q)L/\hbar - n\pi]} - e^{-in\pi/2} \frac{\sin[((p-q)L/\hbar + n\pi)/2]}{[(p-q)L/\hbar + n\pi]} \right\}
\end{aligned} \tag{B1}$$

and we briefly sketch out some of the necessary steps in the evaluation of $P_W^{(n)}(x, p)$ in this approach.

Combining the various complex exponentials and using the fact that the Wigner function must be real, we are left with integrals such as

$$\mathcal{I}_1 = \int_{-\infty}^{+\infty} \cos \left[\frac{qL}{\hbar} \left(\frac{L-2x}{L} \right) \right] \frac{\sin[((p+q)L/\hbar - n\pi)/2]}{[(p+q)L/\hbar - n\pi]} \frac{\sin[((p-q)L/\hbar - n\pi)/2]}{[(p-q)L/\hbar - n\pi]} dq. \tag{B2}$$

In this case, the appropriate partial fraction identity to rewrite the denominators is

$$\frac{1}{((p+q)L/\hbar - n\pi)((p-q)L/\hbar - n\pi)} = \frac{1}{2(pL/\hbar - n\pi)} \left\{ \frac{1}{((p+q)L/\hbar - n\pi)} + \frac{1}{((p-q)L/\hbar - n\pi)} \right\} \tag{B3}$$

and the remaining integrals can be done using variations on Eqn. (40). Upon combining various factors, one obtains integrals of that form not only with $m = (L-2x)/L$, as in Eqn. (39), but similar ones with $m = (L-4x)/L$ and $m = (3L-4x)/L$. These terms give rise to limits on the x dependence of the form $\mathcal{R}(x; 0, L/2)$ and $\mathcal{R}(x; L/2, L)$ where $\mathcal{R}(x; a, b)$ is defined in Eqn. (44). For example, one intermediate result can be written in the form

$$\begin{aligned}
\mathcal{T} &= \cos \left[\left(\frac{pL}{\hbar} - n\pi \right) \left(\frac{L-2x}{L} \right) \right] \sin \left[\left(\frac{pL}{\hbar} - n\pi \right) \right] \mathcal{R}(x; 0, L) \\
&\quad - \sin \left[\left(\frac{pL}{\hbar} - n\pi \right) \left(\frac{L-2x}{L} \right) \right] \cos \left[\left(\frac{pL}{\hbar} - n\pi \right) \right] \{ \mathcal{R}(x; 0, L/2) - \mathcal{R}(x; L/2, L) \}
\end{aligned} \tag{B4}$$

which, in turn, gives

$$\mathcal{T} = \begin{cases} 0 & \text{for } x < 0, x > L \\ \sin[(2(p/\hbar - n\pi/L)x)] & \text{for } 0 < x < L \\ \sin[(2(p/\hbar - n\pi/L)(L-x))] & \text{for } L/2 < x < L \end{cases} \tag{B5}$$

so that the ‘split’ definition of $P_W^{(n)}(x, p)$ in the two half intervals arises very naturally and the complete result in Eqn. (59) is reproduced using momentum-space methods, including the non-trivial x dependence.

APPENDIX C: PROBLEMS

P1: Complete the proof that the $\phi_n(p)$ for the ISW are orthonormal by explicit calculation of $\langle \phi_m | \phi_n \rangle$, completing the steps in Sec. III, and making use of identities such as Eqn. (46).

P2: Using results from any quantum mechanics textbook, evaluate the Wigner distribution for the ground state and first excited state of the simple harmonic oscillator. **Answer:** The harmonic oscillator eigenstates can be written in the form

$$u_n(z) = A_n H_n(z) e^{-z^2/2} \quad \text{where} \quad A_n \equiv \frac{1}{\sqrt{2^n n!} \sqrt{\pi}} \quad \text{and} \quad z \equiv \frac{x}{b} = \frac{x}{\sqrt{\hbar/m\omega}} \quad (\text{C1})$$

and the $H_n(z)$ are the Hermite polynomials of order n . The Wigner functions for $n = 0, 1$ are then given by

$$P_W^{(0)}(x, p) = \frac{1}{\pi \hbar} e^{-\rho^2} \quad (\text{C2})$$

$$P_W^{(1)}(x, p) = \frac{1}{\pi \hbar} e^{-\rho^2} (2\rho^2 - 1) \quad (\text{C3})$$

where

$$\rho^2 \equiv \frac{x^2}{b^2} + \frac{b^2 p^2}{\hbar^2}. \quad (\text{C4})$$

This is one of the simpler results which shows explicitly that the Wigner function need not be positive-definite. Note that the first of these results is consistent with the expression for the free-particle Gaussian in Eqn. (17) for vanishing x_0 , p_0 , and t . The Wigner function for arbitrary n has been evaluated (see, *e.g.*, Ref. [5]) with the result that

$$P_W^{(n)} = \frac{(-1)^n}{\pi \hbar} e^{-\rho^2} L_n(2\rho^2) \quad (\text{C5})$$

where $L_n(z)$ are the Laguerre polynomials.

P3: Show how the phase-space plot for the 1-D harmonic oscillator can be used to generate the classical probability densities for position- and momentum-variables, namely, show how

one obtains

$$P_{CL}(x) = \frac{1}{\pi \sqrt{x_A^2 - x^2}} \quad \text{and} \quad P_{CL}(p) = \frac{1}{\pi \sqrt{p_A^2 - p^2}}. \quad (\text{C6})$$

Partial answer: The classical probability distribution from Eqn. (49) can be written in the form

$$P_{CL}(x, p) \propto \delta(p(x)^2 - p^2) = \frac{1}{2p(x)} [\delta(p(x) - p) + \delta(p(x) + p)] \quad (\text{C7})$$

where

$$p(x) = \sqrt{2mE - m^2\omega^2x^2} = m\omega\sqrt{x_A^2 - x^2}. \quad (\text{C8})$$

Integration of Eqn. (C7) over dp then gives

$$P_{CL}(x) \propto \frac{1}{p(x)} \propto \frac{1}{\sqrt{x_A^2 - x^2}} \quad (\text{C9})$$

which when properly normalized (integrated over the classically allowed interval $(-x_A, +x_A)$) gives the first term in Eqn. (C6).

P4: Using either the momentum- or position-space wavefunctions in Eqns. (13) or (14) for the free-particle Gaussian wave packet, show that the Wigner function is of the form in Eqn. (17).

P5: Complete the proof that the result for the Wigner function for eigenstates of the ISW in Eqn. (59) can be obtained using momentum-space wavefunctions, using the techniques in Appendix B.

P6: Use the results in Eqn. (29) and (62) to write down the time-dependent Wigner function for the simple two-state system in the infinite well

$$\psi(x, 0) = \frac{1}{\sqrt{2}} [u_1(x) + u_2(x)] \quad (\text{C10})$$

and generate plots of $P_W^{(\psi)}(x, p; t)$ for various times. Compare the results to standard images of the position-space and momentum-space probability densities for this problem [46], [47]. What is the only time scale associated with this system? and does it have anything to do with a classical periodicity?

-
- [1] E. Wigner, *On the quantum correction for thermodynamic equilibrium*, Phys. Rev. **40**, 749-759 (1932).
- [2] V. I. Tatarskiĭ, *The Wigner representation of quantum mechanics*, Sov. Phys. Usp. **26**, 311-327 (1983).
- [3] N. L. Balaczs and B. K. Jennings, *Wigner's function and other distribution functions in mock phase space*, Phys. Rep. **105**, 347-391 (1984).
- [4] P. Carruthers and F. Zachariasen, *Quantum collision theory with phase-space distributions*, Rev. Mod. Phys. **55**, 245-285 (1983).
- [5] M. Hillery, R. F. O'Connell, M. O. Scully, and E. P. Wigner, *Distribution functions in physics: Fundamentals*, Phys. Rep. **106**, 121-167 (1984).
- [6] J. Bertrand and P. Bertrand, *A tomographic approach to Wigner's function*, Found. Phys. **17**, 397-405 (1987).
- [7] Y. S. Kim and E. P. Wigner, *Canonical transformations in quantum mechanics*, Am. J. Phys. **58**, 439-448 (1990).
- [8] Y. S. Kim and M. E. Noz, *Phase space picture of quantum mechanics: Group theoretical approach*, Lecture Notes in Physics Series, Vol. 40 (World Scientific, Singapore, 1990)
- [9] H.-W. Lee, *Theory and application of the quantum phase-space distribution functions*, Phys. Rep. **259**, 147-211 (1995).
- [10] A. M. Ozorio de Almeida, *The Weyl representation in classical and quantum mechanics*, Phys. Rep. **296**, 265-342 (1998)
- [11] R. F. O'Connell and E. P. Wigner, *Quantum mechanical distribution functions: Conditions for uniqueness*, Phys. Lett. **83A**, 145-148 (1981).
- [12] R. F. O'Connell and A. K. Rajagopal, *New interpretation of the scalar product in Hilbert space*, Phys. Rev. Lett. **48**, 525-526 (1982).
- [13] R. F. O'Connell and D. F. Walls, *Operational approach to phase-space measurements in quantum mechanics*, Nature **312**, 257-258 (1984).
- [14] W. Schleich, D. F. Walls, and J. A. Wheeler, *Area of overlap and interference in phase space versus Wigner pseudoprobabilities*, Phys. Rev. **A38**, 1177-1186 (1988).
- [15] J. P. Dahl and M. Singborg, *Wigner's phase space function and atomic structure I. The*

- hydrogen atom ground state*, Mol. Phys. **47**, 1001-1019 (1982); M. Springborg and J. P. Dahl, *Wigner's phase space and atomic structure II. Ground states for closed-shell atoms*, Phys. Rev. **A36**, 1050-1062 (1987).
- [16] J. P. Dahl, *Dynamical equations for the Wigner functions*, in *Energy storage and redistribution in molecules*, edited by J. Hinze (Plenum, New York, 1983) pp. 557-572.
- [17] M. Springborg, *Wigner's phase space function and the bond in LiH*, Theoret. Chim. Act (Berl.) **63**, 349-356 (1983).
- [18] J. P. Dahl and M. Springborg, *The Morse oscillator in position space, momentum space, and phase space*, J. Chem. Phys. **88**, 4535-4537 (1988).
- [19] M. Hug, C. Menke, and W. P. Schleich, *Modified spectral method in phase space: Calculation of the Wigner function. I. Fundamentals*, Phys. Rev. **A57**, 3188-3205 (1988); *Modified spectral method in phase space: Calculation of the Wigner function. II. Generalizations*, Phys. Rev. **A57**, 3188-3205 (1988).
- [20] J. Snygg, *Wave functions rotated in phase space*, Am. J. Phys. **45**, 58-60 (1977).
- [21] N. Mukunda, *Wigner distribution for angle coordinates in quantum mechanics*, Am. J. Phys. **47**, 192-187 (1979).
- [22] S. Stenholm, *The Wigner function: I. The physical interpretation*, Eur. J. Phys. **1**, 244-248 (1980).
- [23] G. Mourgues, J. C. Andrieux, and M. R. Feix, *Solution of the Schroedinger equation for a system excited by a time Dirac pulse of potential. An example of the connection with the classical limit through a particular smoothing of the Wigner function*, Eur. J. Phys. **5**, 112-118 (1984).
- [24] M. Casas, H. Krivine, and J. Martorell, *On the Wigner transforms of some simple systems and their semiclassical interpretations*, Eur. J. Phys. **12**, 105-111 (1991).
- [25] R. A. Campos, *Correlation coefficient for incompatible observables of the quantum harmonic oscillator*, Am. J. Phys. **66**, 712-718 (1998).
- [26] I. Bialynicki-Birula, M. Cieplak, and J. Kaminski, *Theory of quanta*, (Oxford University Press, New York, 1992).
- [27] L. E. Ballentine, *Quantum mechanics: A modern development*, (World Scientific, Singapore, 1998).
- [28] L. Cohen, *Time-frequency analysis*, (Prentice-Hall, Englewood Cliffs, 1995).

- [29] M. O. Scully and M. Suhail Zubairy, *Quantum optics*, (Cambridge University Press, Cambridge, 1997).
- [30] W. P. Schleich, *Quantum optics in phase space*, (Wiley-VCH, Berlin, 2001).
- [31] W. Kinzel, *Bilder elementarer Quantenmechanik*, Phys. Bl. **51**, 1190-1191 (1995).
- [32] M. V. Berry, *Quantum fractals in boxes*, J. Phys. A: Math. Gen. **29**, 6617-6629 (1996).
- [33] F. Großmann, J. -M. Rost, and W. P. Schleich, *Spacetime structures in simple quantum systems*, J. Phys. **A30**, L277-L283 (1997).
- [34] P. Stifter, C. Leichtle, W. P. Schleich, and J. Marklov, *Das Teilchen im Kasten: Strukturen in der Wahrscheinlichkeitsdichte* (translated as *The particle in a box: Structures in the probability density*), Z. Naturforsch **52 a**, 377-385 (1997).
- [35] I. Marzoli, F. Saif, I. Bialynicki-Birula, O. M. Friesch, A. E. Kaplan, W. P. Schleich, *Quantum carpets made simple*, Acta Phys. Slov. **48**, 323-333 (1998) [arXiv:quant-ph/9806033].
- [36] A. E. Kaplan, P. Stifter, K. A. H. van Leeuwen, W. E. Lamb, Jr., and W. P. Schleich, *Intermode traces – Fundamental interference phenomena in quantum and wave physics*, Phys. Scr. **T76**, 93-97 (1998).
- [37] W. Loinaz and T. J. Newman, *Quantum revivals and carpets in some exactly solvable systems*, J. Phys. A: Math. Gen. **32**, 8889-8895 (1999) [arXiv:quant-ph/9902039].
- [38] M. J. W. Hall, M. S. Reineker, W. P. Schleich, *Unravelling quantum carpets: a travelling wave approach*, J. Phys. **A32**, 8275-8291 (1999) [arXiv:quant-ph/9906107].
- [39] A. E. Kaplan, I. Marzoli, W. E. Lamb, Jr., and W. P. Schleich, *Multimode interference: Highly regular pattern formation in quantum wave-packet evolution*, Phys. Rev. **A61**, 032101 (2000).
- [40] O. M. Friesch, I. Marzoli, and W. P. Schleich, *Quantum carpets woven by Wigner functions*, New. J. Phys. **2**, 4.1-4.11 (2000) <http://www.iop.org/EJ/journal/JNP>. Video sequences of time-dependent Wigner function for the infinite well are presented at this Web site.
- [41] R. Bluhm, V. A. Kostelecký, and J. Porter, *The evolution and revival structure of localized quantum wave packets*, Am. J. Phys. **64**, 944-953 (1996) [arXiv:quant-ph/9510029].
- [42] R. W. Robinett, *Quantum wave packet revivals*, to appear in Physics Reports.
- [43] A positive definite quasi-probability distribution can be obtained by the use of a Gaussian ‘smearing’ function in the definitions in Eqns. (4) or (5), which gives rise to the so-called Husimi function [5], [9], [27], $P_H(x, p; t)$. This quasi-probability density, however, does not give the correct marginal distributions as in Eqns. (7) and (8).

- [44] R. L. Hudson, *When is the Wigner quasi-probability density non-negative?*, Rep. Math. Phys. **6** 249-252 (1974); F. Soto and P. Claverie, *When is the Wigner function of multi-dimensional systems nonnegative?*, J. Math. Phys. **24**, 97-100 (1983).
- [45] CRC Standard Mathematical Tables, (CRC Press, Cleveland, 2000).
- [46] R. W. Robinett, *Quantum mechanics: Classical results, modern systems, and visualized examples*, (Oxford, New York, 1997), pp. 123-126.
- [47] One of the earliest pedagogical visualizations of the time dependence of such a two-state system is by C. Dean, *Simple Schrödinger wave functions which simulate classical radiating systems*, Am. J. Phys. **27**, 161-163 (1959).
- [48] M. Born, *Continuity, determinism, and reality*, Kgl. Danske Videns. Sels. Mat.-fys. Medd., **30** (2), (1955) 1-26. Born was addressing concerns made by Einstein in *Elementare Überlegungen zur Interpretation der Grundlagen der Quanten-Mechanik*, in *Scientific papers presented to Max Born* (Oliver and Boyd, Edinburgh, 1953) pp. 33-40.
- [49] M. A. Doncheski, S. Heppelmann, R. W. Robinett, and D. C. Tussey, *Wave packet construction in two-dimensional quantum billiards: Blueprints for the square, equilateral triangle, and circular cases*, Am. J. Phys. **71**, 541-557 (2003) [arXiv:quant-ph/0307070].
- [50] R. W. Robinett, *Visualizing the collapse and revival of wave packets in the infinite square well using expectation values*, Am. J. Phys. **68**, 410-42 (2000) [arXiv:quant-ph/0307041].
- [51] M. Kleber, *Exact solutions for time-dependent phenomena in quantum mechanics*, Phys. Rep. **236** 331-393 (1994).
- [52] M. Andrews, *Wave packets bouncing off walls*, Am. J. Phys. **66** 252-254 (1998).
- [53] D. L. Aronstein and C. R. Stroud, Jr., *Fractional wave-function revivals in the infinite square well*, Phys. Rev. **A55** 4526-4537 (1997).
- [54] I. Sh. Averbukh and N. F. Perelman, *Fractional revivals: Universality in the long-term evolution of quantum wave packets beyond the correspondence principle dynamics*, Phys. Lett. **A139**, 449-453 (1989); *Fractional revivals of wave packets*, Acta Phys. Pol. **78**, 33-40 (1990). This paper includes much of the material in the citation above, correcting some minor typographical errors; *Fractional regenerations of wave-packets in the course of long-term evolution of highly excited quantum-systems*, Zh. Eksp. Teor. Fiziki. **96**, 818-827 (1989) (Sov. Phys. JETP **69**, 464-469 (1989).)
- [55] M. A. Doncheski and R. W. Robinett, *Comparing classical and quantum probability distribu-*

- tions for an asymmetric well*, Eur. J. Phys. **21**, 217-228 (2000).
- [56] A. Bonvalet, J. Nagle, V. Berger, A. Migus, J. -L. Martin, and M. Joffre, *Femtosecond infrared emission resulting from coherent charge oscillations in quantum wells*, Phys. Rev. Lett. **76**, 4392-4395 (1996).
- [57] M. A. Doncheski and R. W. Robinett, *Anatomy of a quantum 'bounce'*, Eur. J. Phys. **20** 29-37 (1999) [arXiv:quant-ph/0307010].

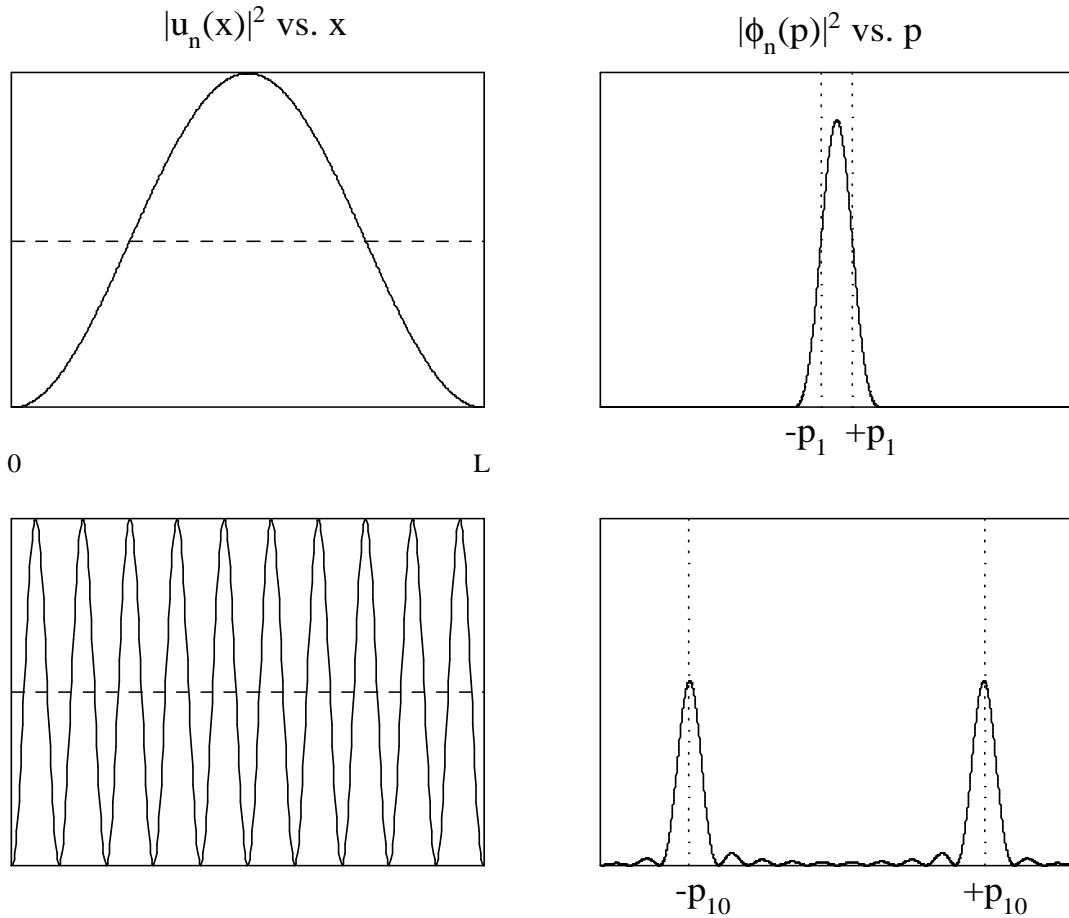


FIG. 1: Plots of the position-space probability density, $|u_n(x)|^2$ versus x , (left) and momentum-space probability density, $|\phi_n(p)|^2$ versus p , (right) for energy eigenstates in the infinite square well for $n = 1$ (top) and $n = 10$ (bottom) cases. The horizontal dashed lines on the left correspond to the (classical) flat probability density given by $P_{CL}(x) = 1/L$ from Eqn. (54), while the vertical dotted lines on the right correspond to the δ -function classical distribution in Eqn. (52).

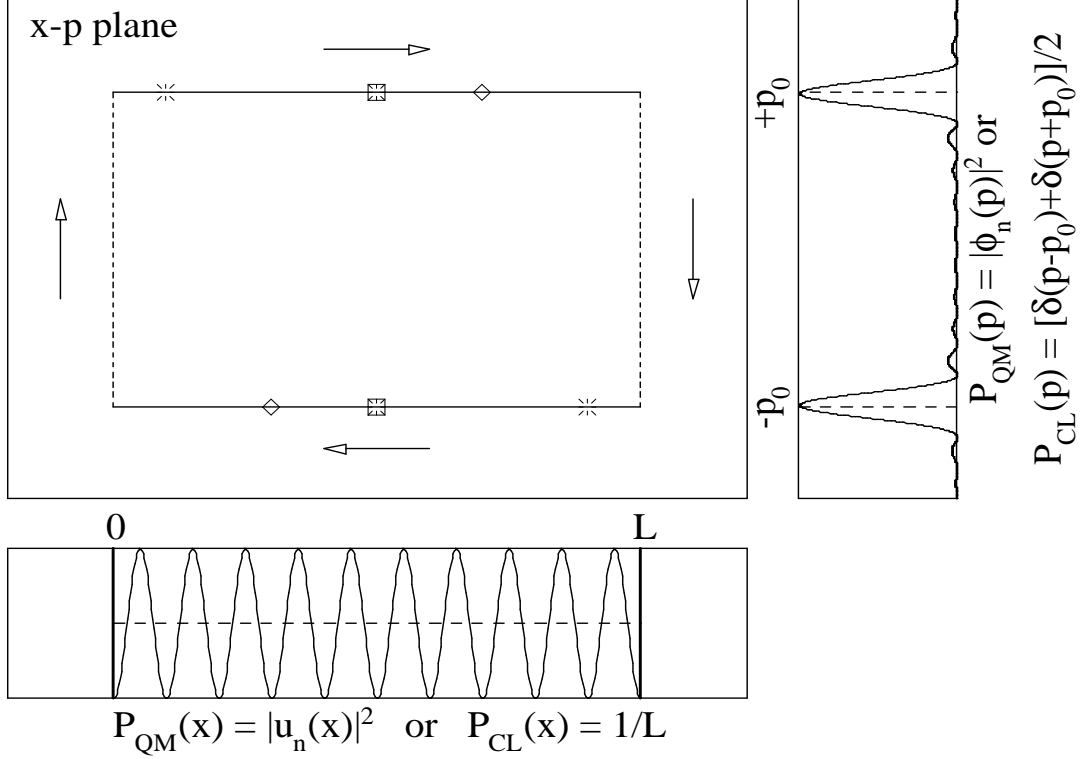


FIG. 2: Classical phase-space picture of solutions of the infinite square well. The classical phase-space trajectory has the particle moving with constant speed (momenta given by $\pm p_0$) between the walls at $x = 0, L$ (solid horizontal lines) with discontinuous changes in velocity (momentum) due to the collisions with the walls (dashed vertical lines). Projections onto the x - and p -axes give the classical probability densities in Eqns. (52) and (54). These are compared with the quantum counterparts, $P_{QM}(x) = |u_n(x)|^2$ versus x , and $P_{QM}(p) = |\phi_n(p)|^2$ versus p , for the case $n = 10$. The pairs of points in phase space indicated by squares (stars, diamonds) are separated in time by half a classical period.

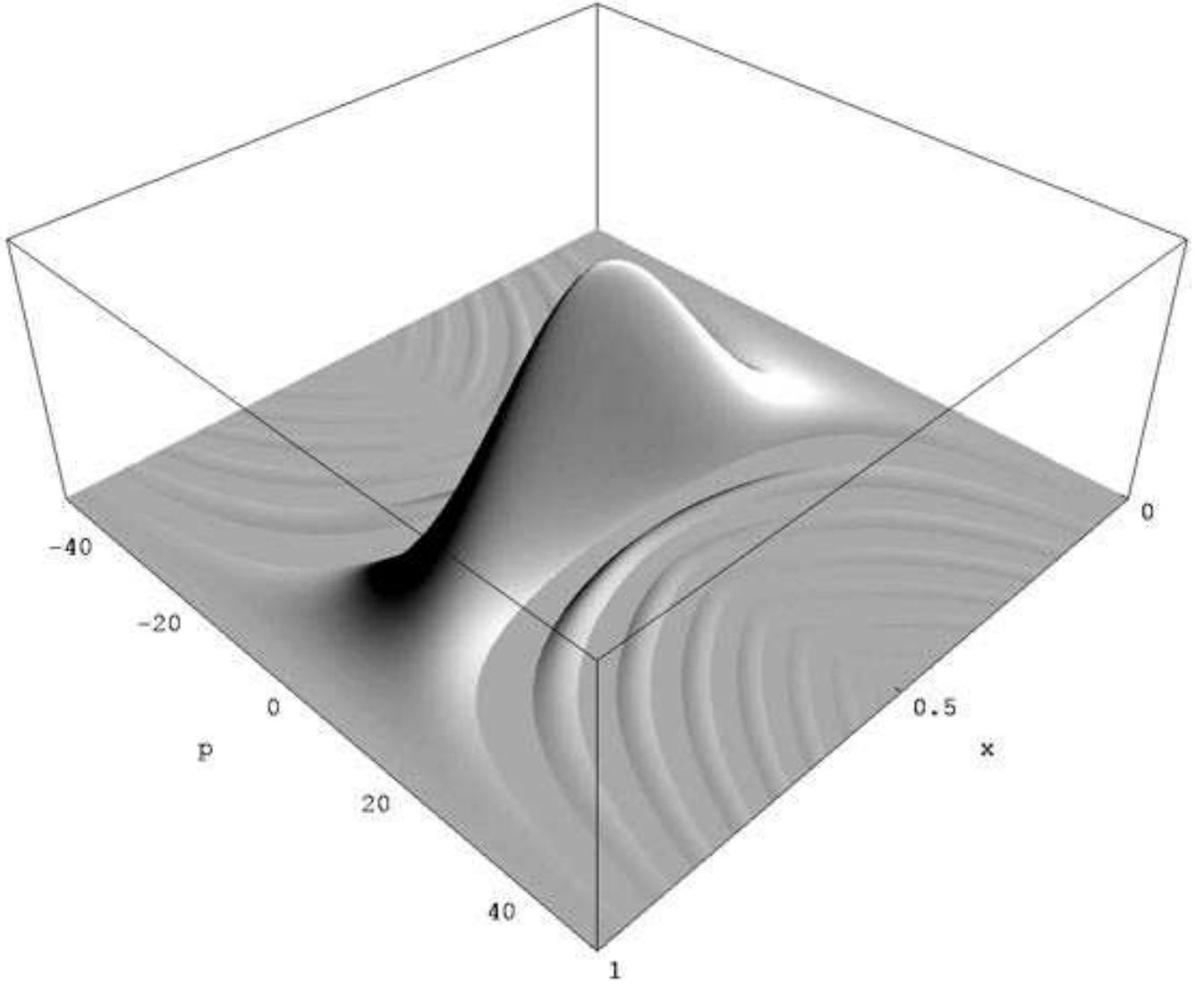


FIG. 3: Plot of the Wigner distribution from Eqn. (59) for the $n = 1$ energy eigenstate in the infinite square well. Only the positive ($P_W^{(1)}(x, p) > 0$) parts are shown.

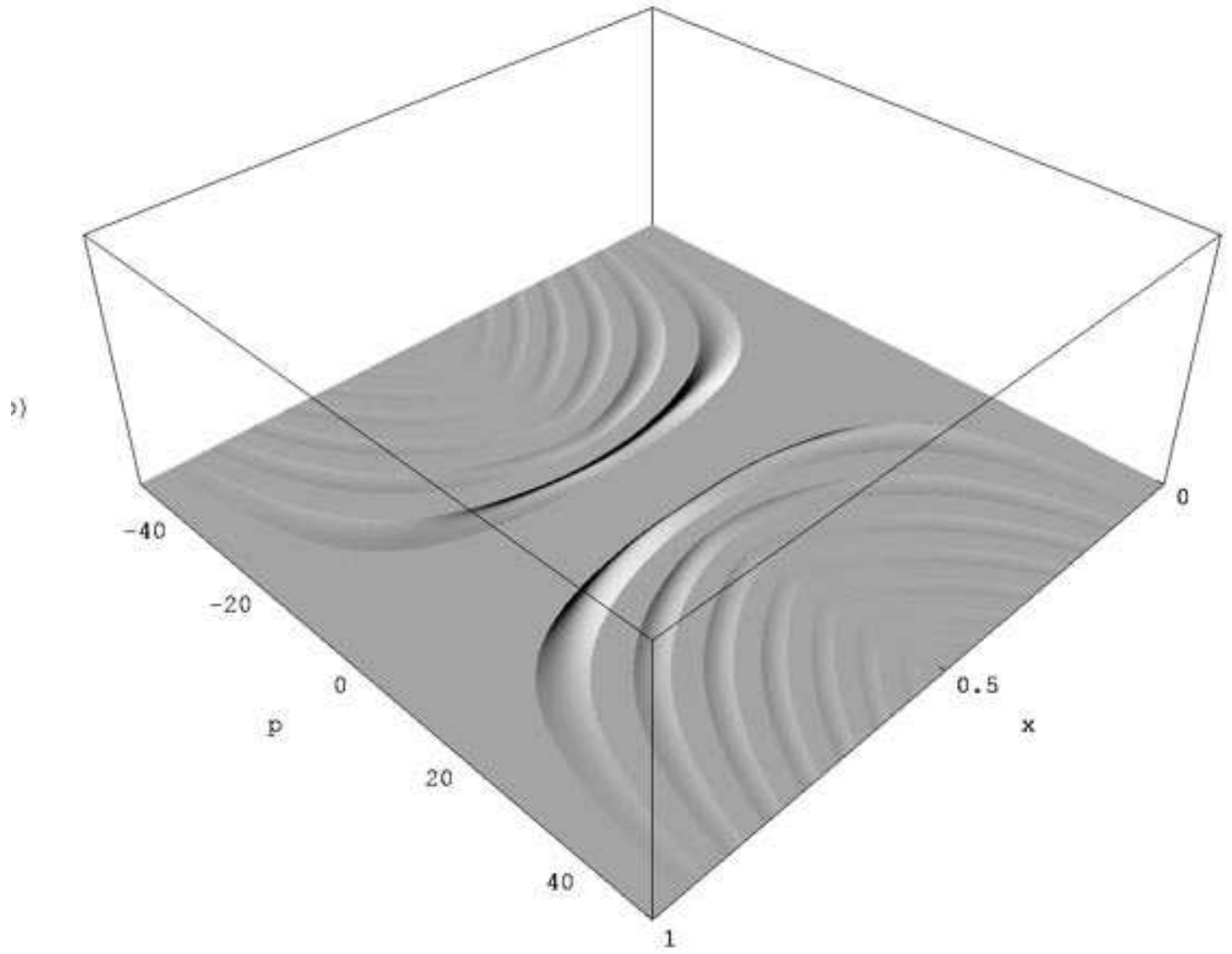


FIG. 4: Same as Fig. 3, but with only the negative ($-P_W^{(1)}(x, p) > 0$) parts shown. This shows that the Wigner function for the ground state of the infinite well is almost, but not quite, positive definite.

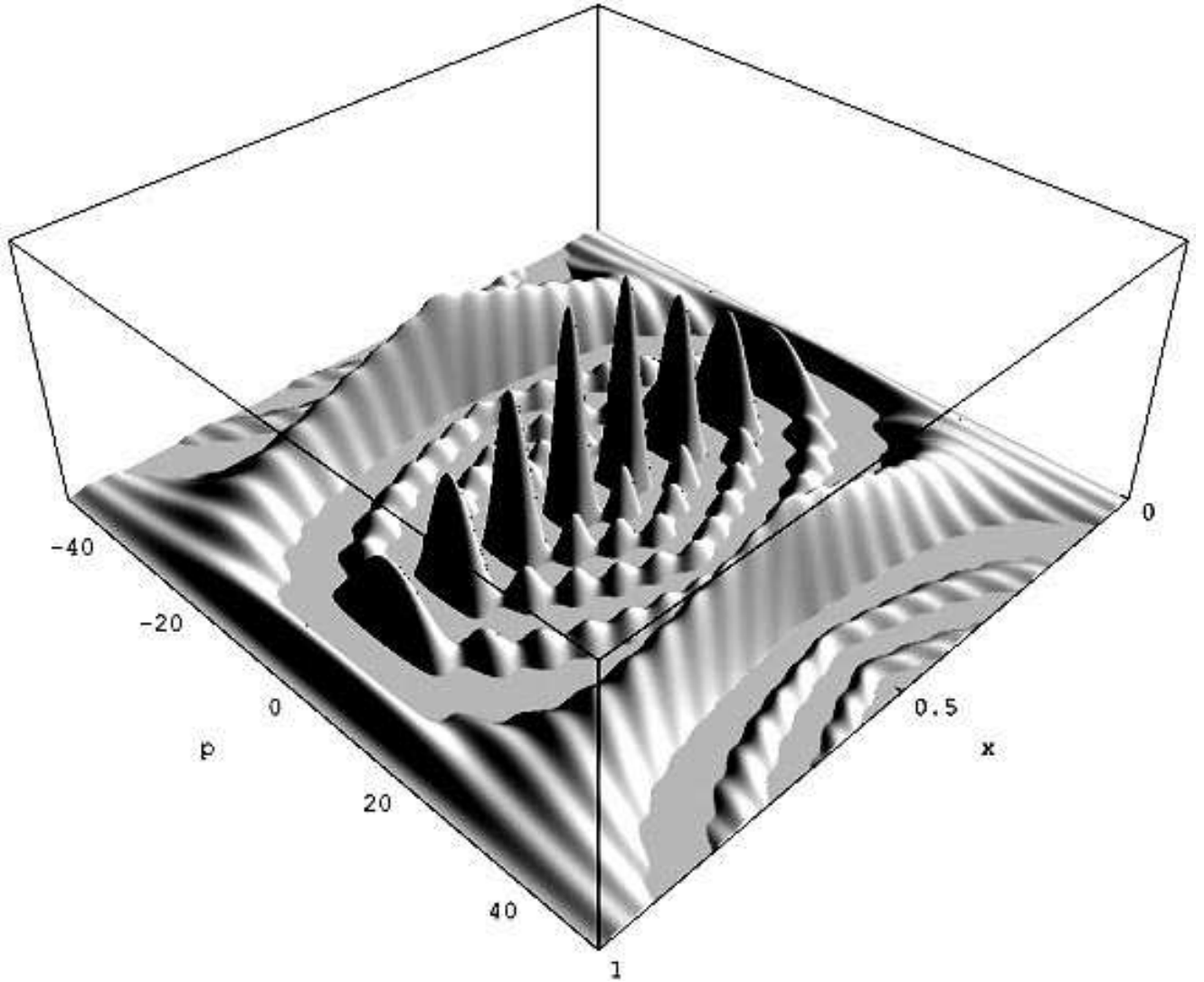


FIG. 5: Plot of the Wigner distribution from Eqn. (59) for the $n = 10$ energy eigenstate in the infinite square well. Only the positive ($P_W^{(10)}(x, p) > 0$) parts are shown.

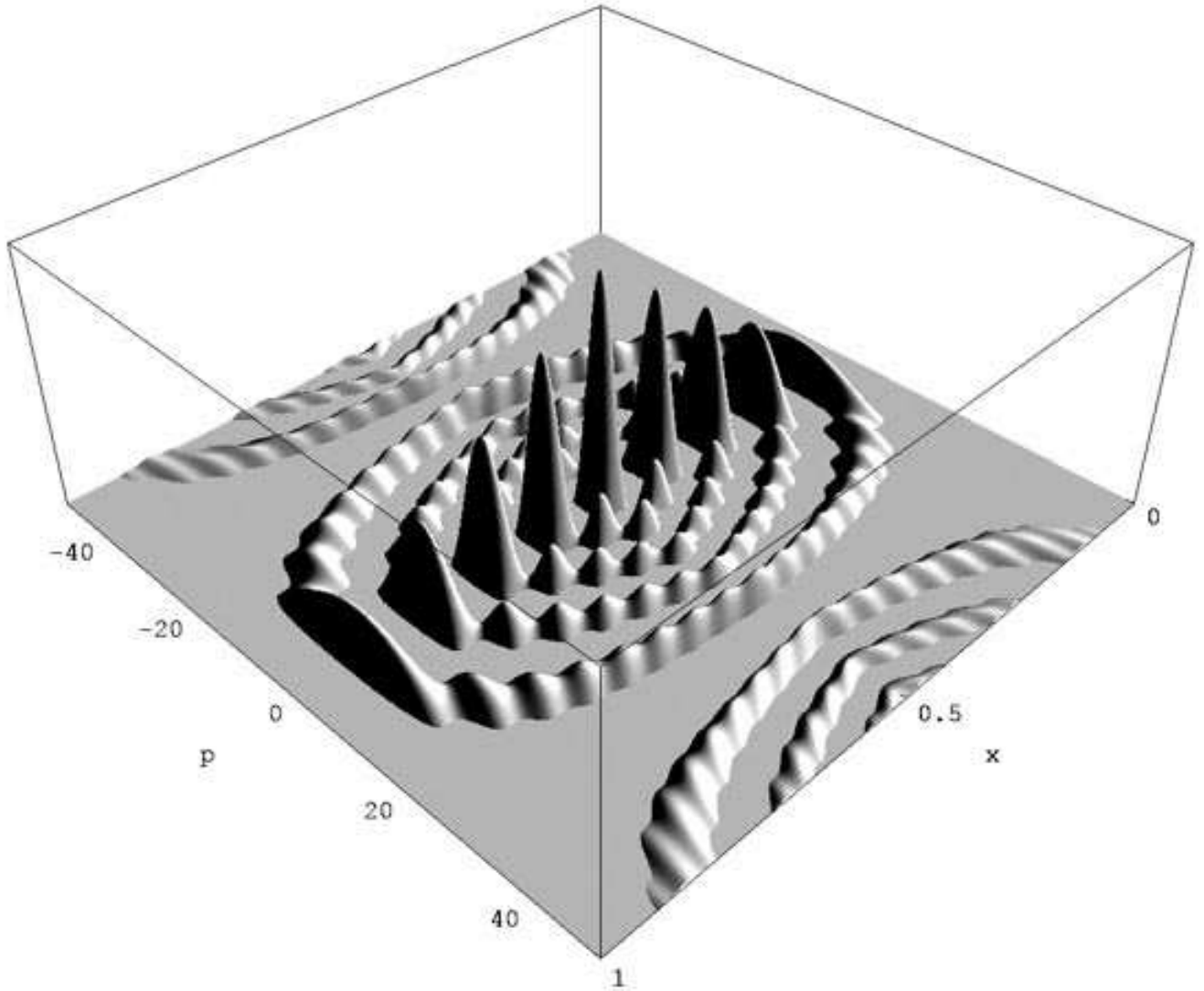


FIG. 6: Same as Fig. 5, but with only the negative ($-P_W^{(10)}(x, p) > 0$) parts shown.

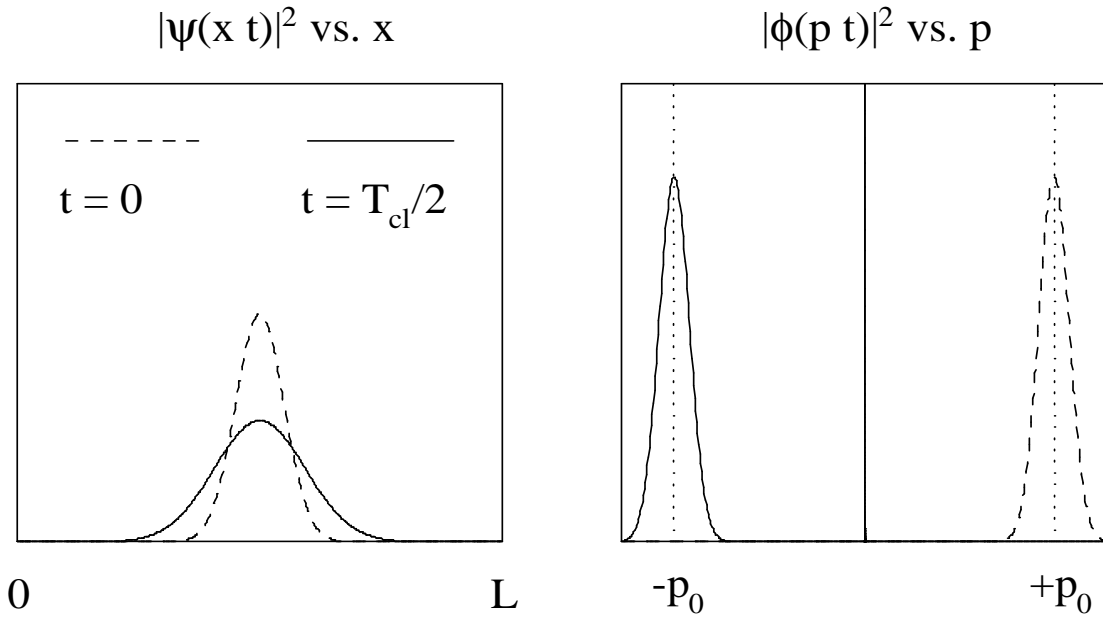


FIG. 7: Plots of the position-space probability density, $|\psi(x,t)|^2$ versus x , and momentum-space probability density, $|\phi(p,t)|^2$ versus p , for a Gaussian wave packet solution in the ISW. Times corresponding to $t = 0$ (dashed) and $T_{cl}/2$ (solid) are shown. The parameters of Eqn. (69) and $n_0 = 40$ are used.

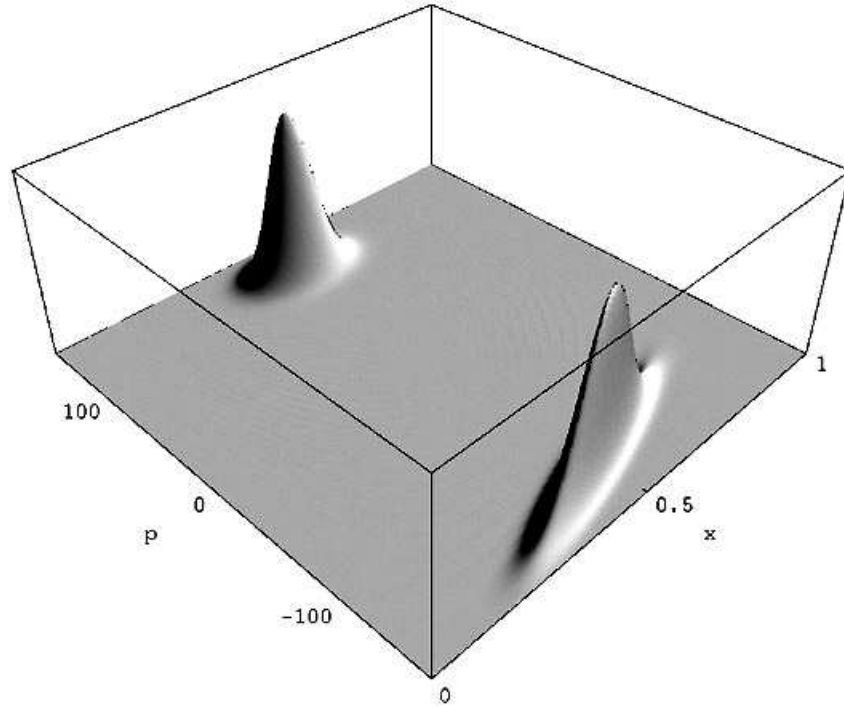


FIG. 8: Plot of the Wigner function, $P_W(x, p; t)$ versus (x, p) as a function of time for $t = 0$ and $t = T_{cd}/2$, to be compared to Fig. 7.

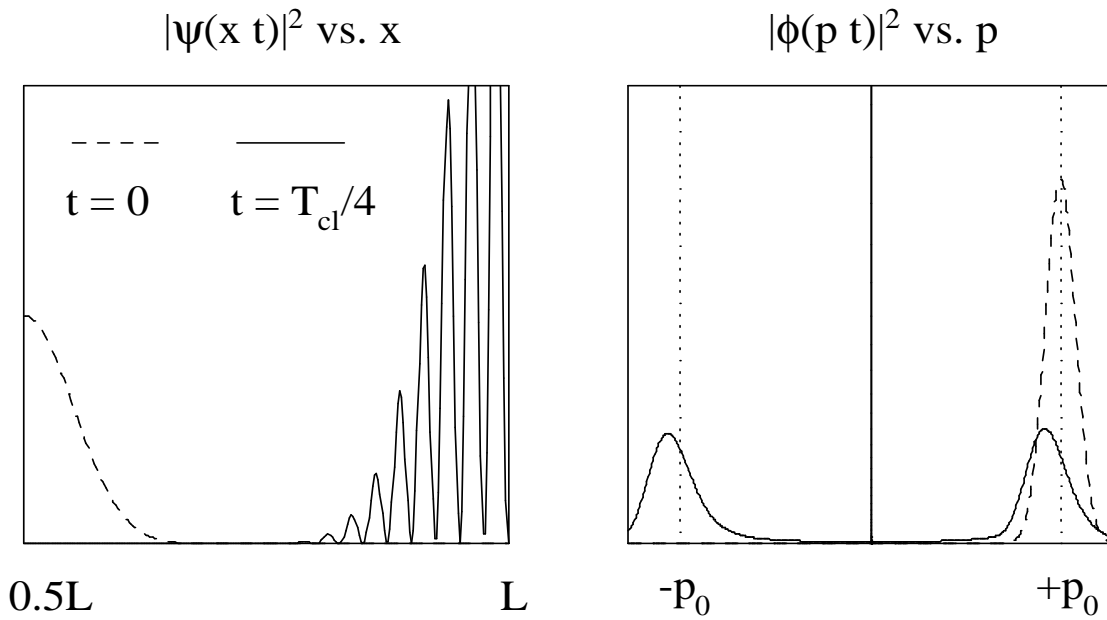


FIG. 9: Same as Fig. 7, except for $t = 0$ (dashed) and $t = T_{cl}/4$ where the classical particle would be hitting the wall. (Recall that the two momentum peaks for the ‘collision’ time are not symmetrically placed at $\pm p_0$ [57] since the high-momentum components of the initial wave packet arrive at the wall, and hence are also reflected, first.) Note that the $|\psi(x,t)|^2$ is plotted over the interval $[L/2, L]$ to show the collision with the wall in more detail.

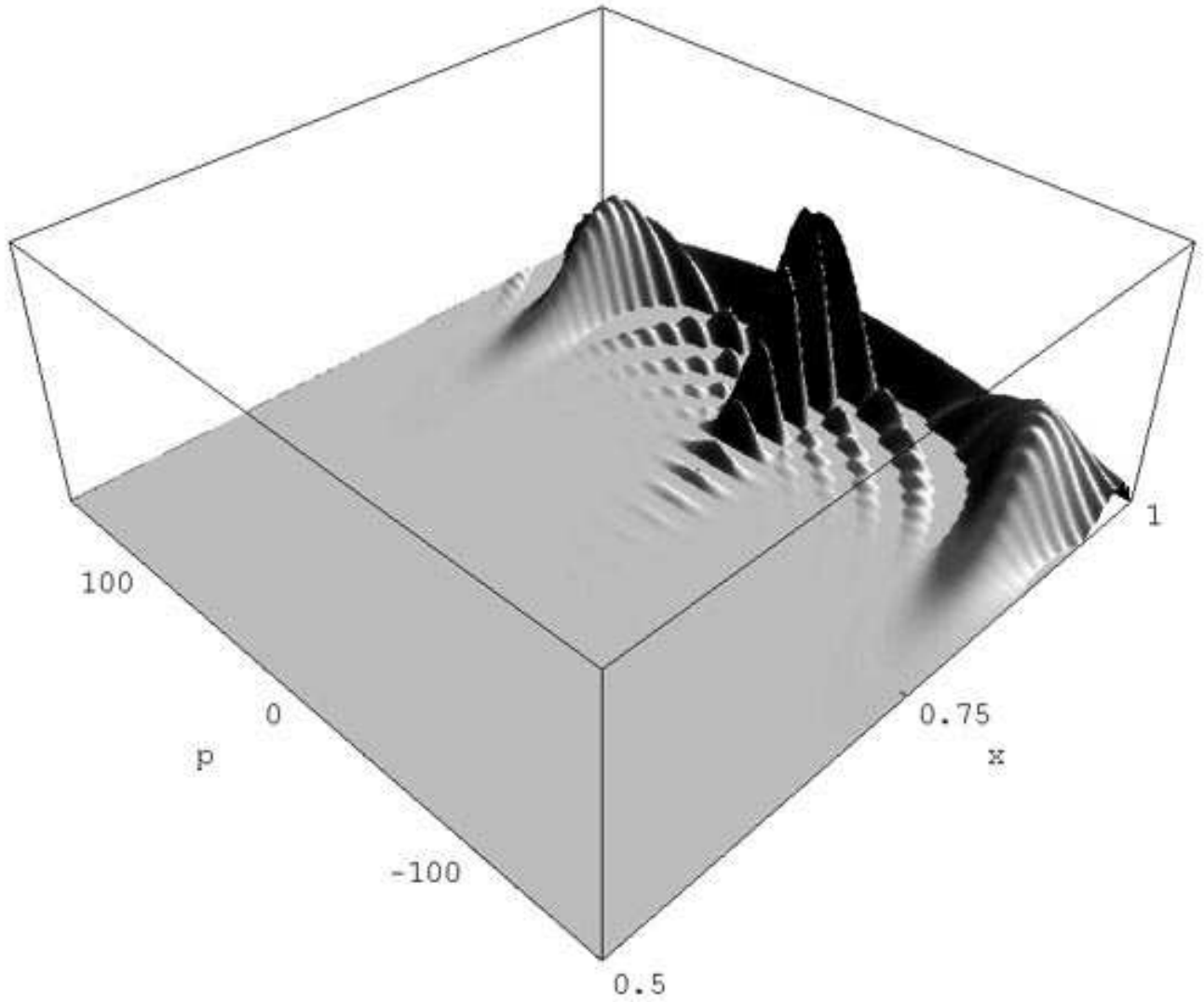


FIG. 10: Same as Fig. 8, but for $t = T_{cl}/4$ where the classical particle would be hitting the wall. Only positive values ($P_W(x, p; t) > 0$) are shown and the x interval $[L/2, L]$ is used, as in Fig. 9.

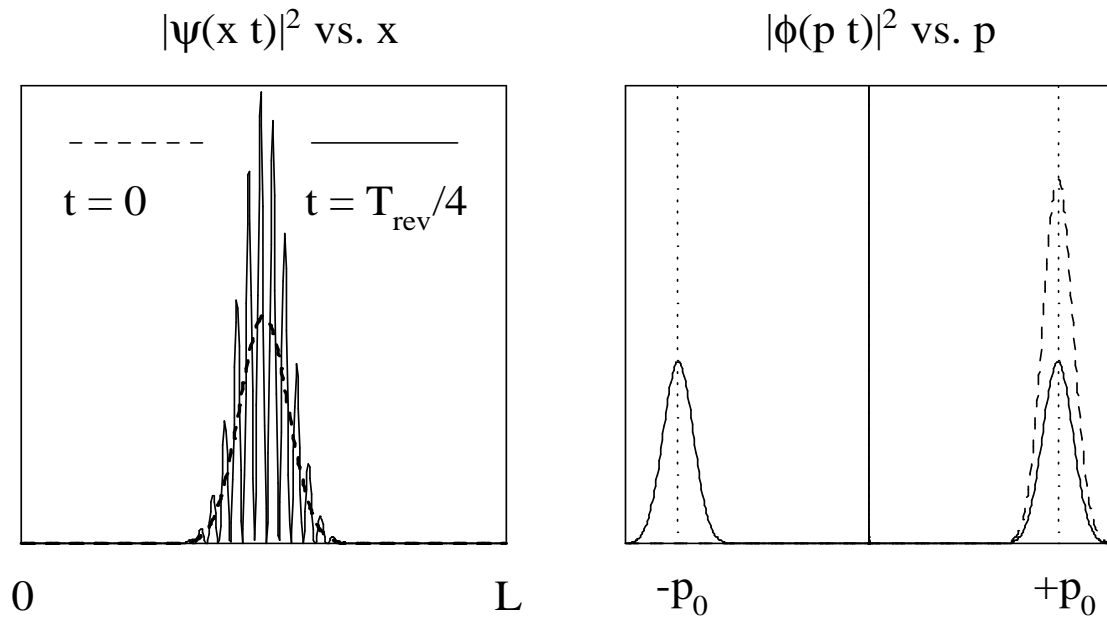


FIG. 11: Same as Fig. 7, except for $t = 0$ (dashed) and for a fractional revival at $t = T_{\text{rev}}/4$ (dashed)

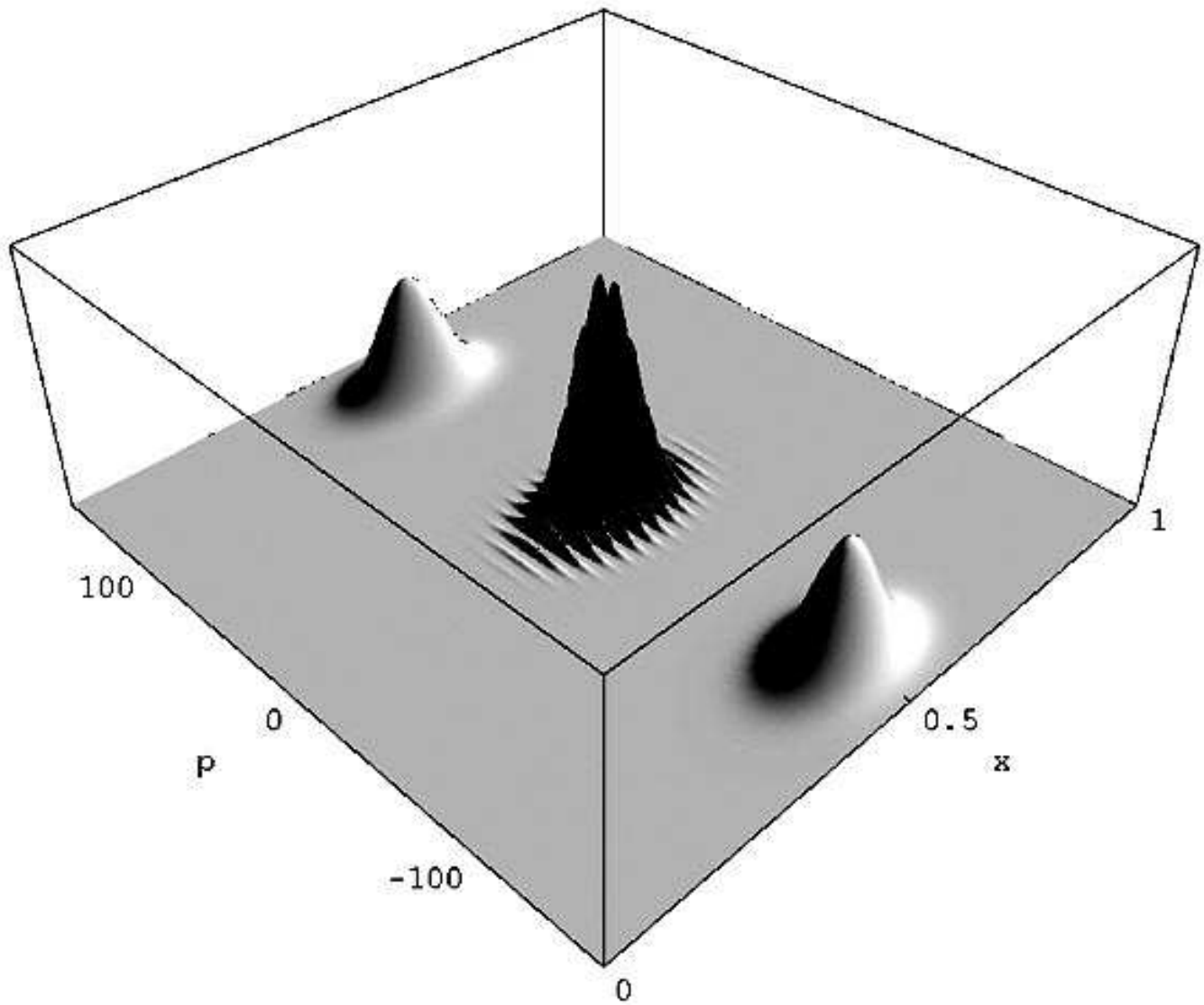


FIG. 12: Same as Fig. 8, but for the fractional revival at $t = T_{rev}/4$, to be compared to Fig. 11. Only positive values ($P_W(x, p; t) > 0$) are shown.

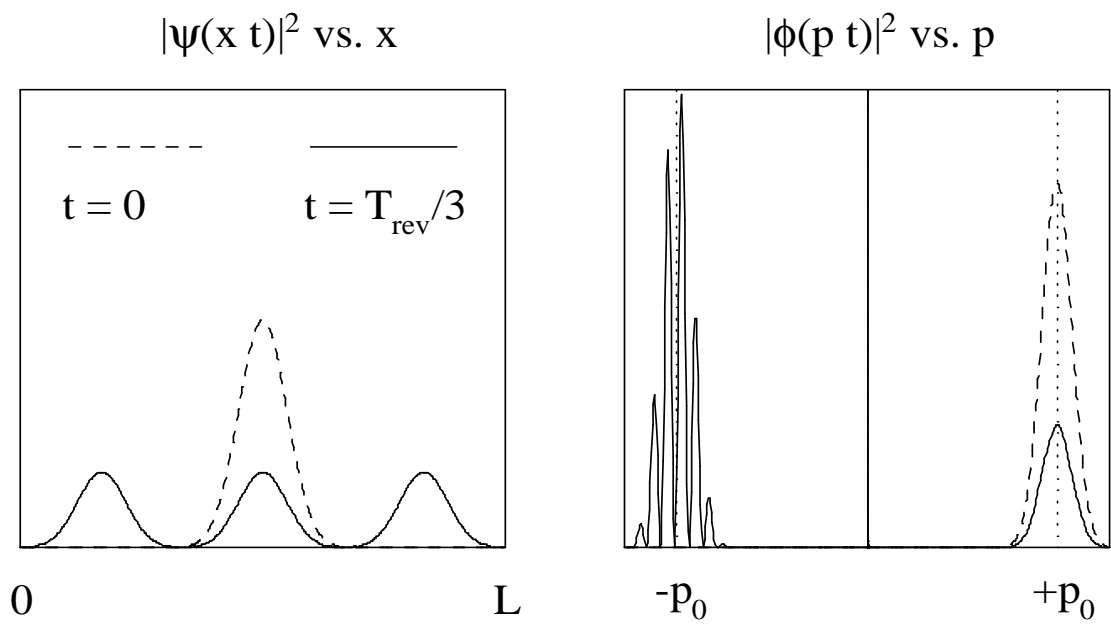


FIG. 13: Same as Fig. 7, except for $t = 0$ (dashed) and for a fractional revival at $t = T_{rev}/3$ (solid).

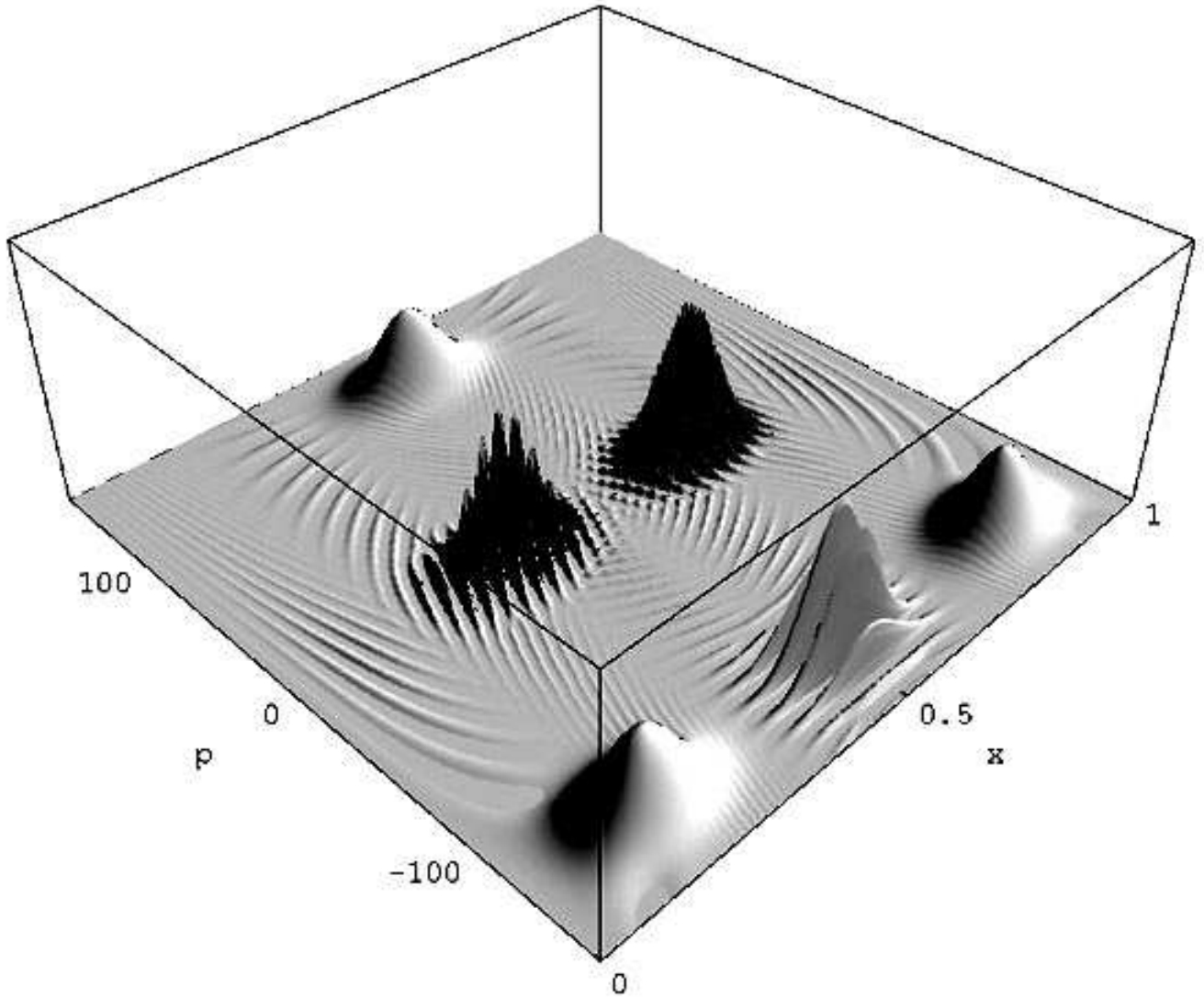


FIG. 14: Same as Fig. 8, but for the fractional revival at $t = T_{rev}/3$, to be compared to Fig. 13. Only positive values ($P_W(x, p; t) > 0$) are shown.

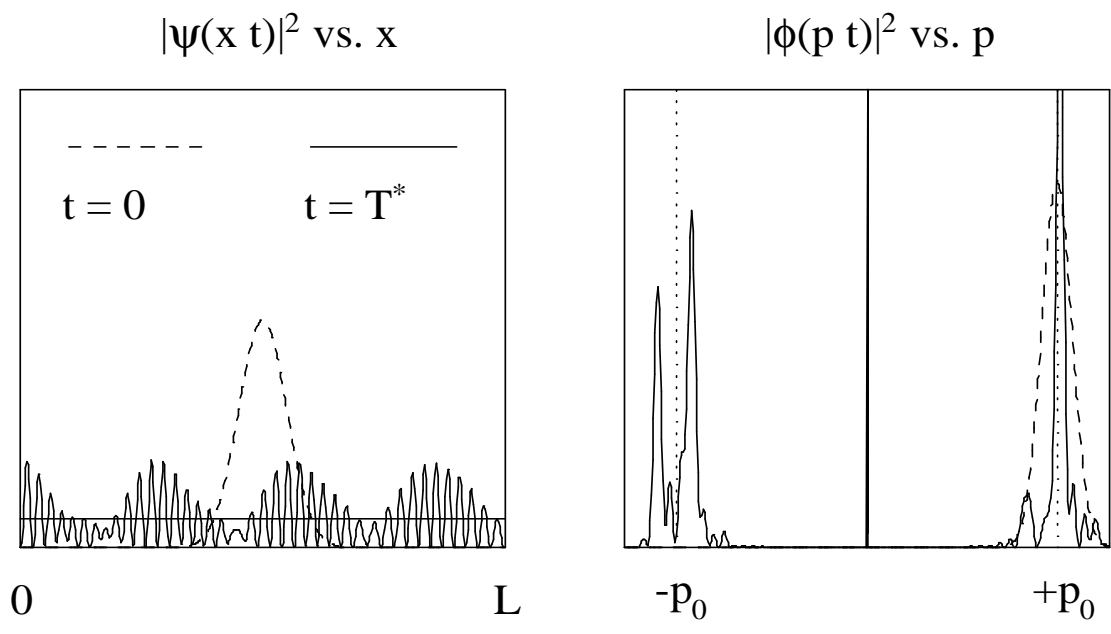


FIG. 15: Same as Fig. 7, except for $t = 0$ (dashed) and for a general time, $T^* = 16T_{rev}/37$ (solid), during the collapsed phase, not near any resolvable fractional revival.

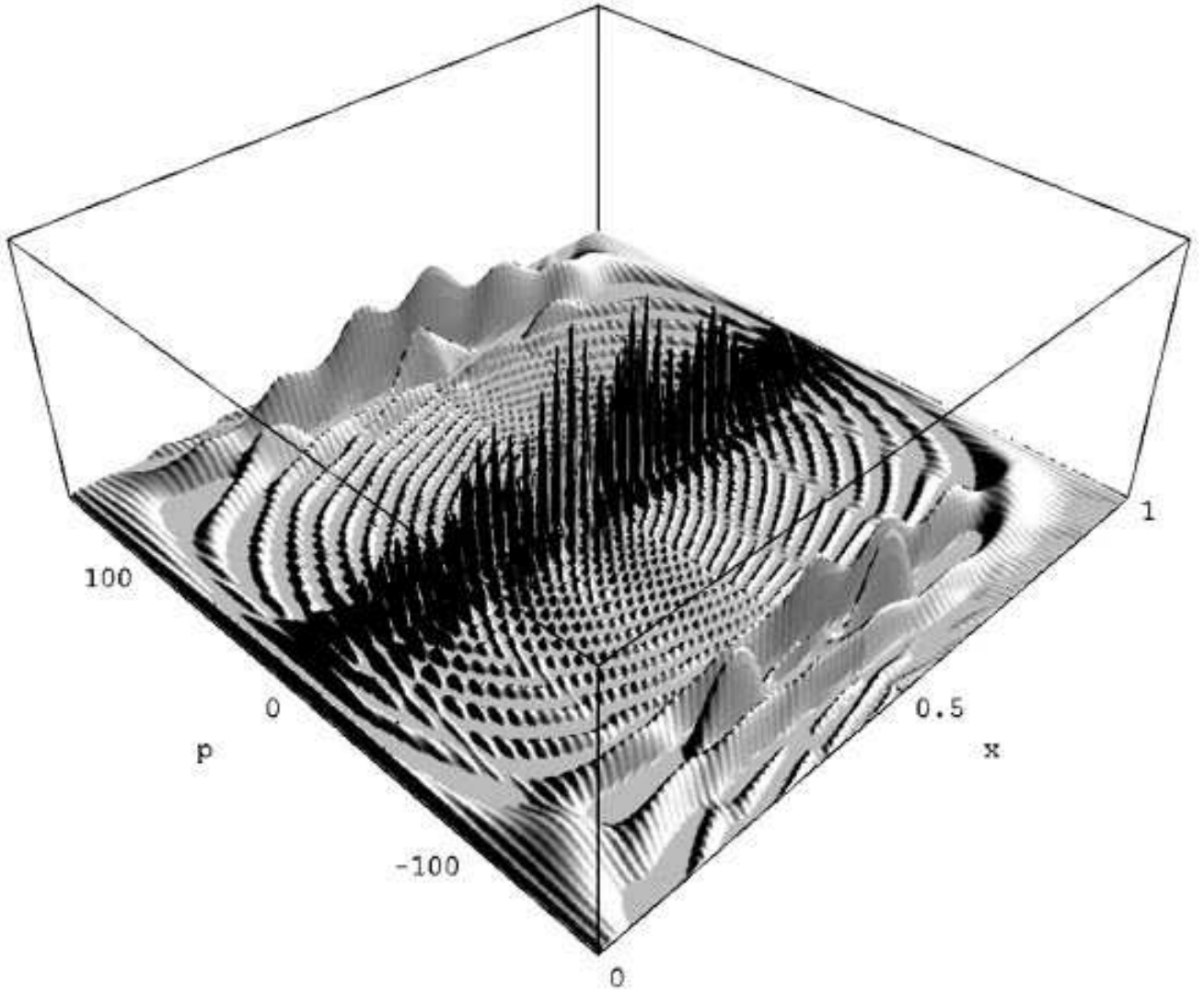


FIG. 16: Same as Fig. 8, but for a general time ($T^* = 16T_{rev}/37$) during the collapsed phase, not near any resolvable fractional revival, to be compared to Fig. 15. Only positive values ($P_W(x, p; t) > 0$) are shown.